Project No:
764697

Project acronym:
CHEERS

Project full title:
Chinese-European Emission-Reducing Solutions

Type of Action: **RIA**

Call/Topic:
European Horizon 2020 Work Programme 2016 – 2017, 10. 'Secure, Clean and Efficient Energy', under the low-carbon energy initiative LCE-29-2017: *CCS in Industry, including BioCCS*

Start-up: 2017-10-01
Duration: 60 months

Deliverable
D5.1: CLC reactor-unit modelling

Due submission date: 2019-09-01

Actual delivery date: 2020-09-01

Organisation name of lead beneficiary for this deliverable:
IFP Energies nouvelles

Project funded by the European Union's Horizon 2020 research and innovation programme under grant agreement No 764697, and co-funded by the Chinese Ministry of Science and Technology (MOST)		
Dissemination Level		
PU	Public	X
CO	Confidential, only for members of the consortium (including the Commission Services and MOST)	
INT	Confidential, only for members of the consortium	

Deliverable number:	D5.1
Deliverable title:	CLC reactor-unit modelling
Deliverable description:	The deliverable includes three parts: a) Definition of design basis for the industrial unit, b) CLC reactor-unit modelling c) Characterisation and performance modelling of oxygen carriers
Work package:	WP5
Lead participant:	IFPEN

Revision Control (only when a submitted deliverable is revised)			
Revision	Date	Author(s)	Comments

Quality assurance, status of deliverable		
Action	Performed by	Date
Delivered (Main author)	Airy TILLAND, Rahul ANANTHARAMAN	2020-07-07
Verified (Work Package leader)	Stéphane BERTHOLIN (IFPEN)	2020-09-02
Approved (Management Support Team)	By e-mail	2020-09-23
Endorsed (Executive Board)	By e-mail	2020-10-12
Submitted to the European Commission	Nils Haugen (SINTEF ER)	2020-10-12

Author(s)		
Name	Organisation	E-mail address (optional)
Catherine LAROCHE	IFPEN	catherine.laroche@ifpen.fr
Airy TILLAND	IFPEN	airy.tiland@ifpen.fr
Tiago SOZINHO	IFPEN	Tiago.sozinho@ifpen.fr
Adriana REYES LÚA	SINTEF ER	adriana.r.lua@sintef.no
Donghoi KIM	SINTEF ER	Donghoi.Kim@sintef.no
Vidar T. SKJERVOLD	SINTEF ER	VidarTorarin.Skjervold@sintef.no
Rahul ANANTHARAMAN	SINTEF ER	Rahul.Anantharaman@sintef.no

Abstract for publication on the website of CHEERS

CHEERS conforms to the European Horizon 2020 Work Programme 2016 – 2017, 10. 'Secure, Clean and Efficient Energy', under the low-carbon energy initiative (LCE-29-2017: CCS in Industry, including BioCCS). The ambition is to improve the efficacy of CO2 capture in industry, and help ensuring sustainable, secure, and affordable energy.

The action involves a 2nd generation chemical-looping technology tested and verified at laboratory scale (150 kWth). Within the framework of CHEERS, the core technology will be developed into a 3 MWth system prototype for demonstration in an operational environment. This constitutes a major step towards large-scale decarbonisation of industry, offering a considerable potential for retrofitting industrial combustion processes.

The system prototype is based on a fundamentally new fuel-conversion process synthesised from prior research and development actions over more than a decade. The system will include heat recovery steam generation with CO_2 separation and purification, and it will comply with industrial standards, specifications and safety regulations. Except for CO_2 compression work, the innovative concept is capable of removing 96 % of the CO_2 while eliminating capture losses to almost zero.

The CHEERS project is financed by the European Union's Horizon 2020 research and innovation programme under grant agreement No 764697, and co-funded by the Chinese Ministry of Science and Technology (MOST).

CHEERS started 1 October 2017 and is scheduled to end by September 2022. The estimated budget is 16 mill. EUR.

The deliverable D5.1 aims at providing the design basis to be considered for the scale-up of the process and the modelling tools to predict the performances of the CLC reactor system. It includes three independent parts :

a) ***Definition of design basis for the industrial unit*** basically provides the application cases that will be considered for the assessment of the CLC technology.
b) ***CLC reactor-unit modelling*** consists in a kinetic and hydrodynamic simulator to predict performances of the Fuel reactor, i.e. the petcoke conversion accounting for various operating conditions such as temperature, steam content in feeding gas, reactor geometry, oxygen carrier and petcoke flowrates and properties, etc.. This model is the result of a multi-scale strategy starting from experimentation in fixed bed and batch fluidized bed reactor to calibrate the kinetic laws. Then, tests in continuous bubbling fluidized bed reactor are predicted with the model to validate the kinetics determined in batch unit. Finally, new correlations are proposed to account for the change of hydrodynamic in the CHEERS demonstration unit and industrial scale units which are operated in turbulent mode instead of bubbling mode.
c) ***Characteristics and performance modelling of oxygen carriers*** presents a framework to find the potential heat recovery from Chemical Looping Combustion (CLC) using different oxygen carriers, based on thermodynamic equilibrium calculations. An equilibrium model based on the minimization of the Gibbs free energy is validated and used to conduct a parametric analysis of the flue gas composition from the CLC fuel reactor using four different oxygen carriers under different process conditions. As the results of this framework are independent of the configuration of the CLC reactor, this tool can aid in the preliminary evaluation of oxygen carriers with potential for CLC applications and relevant operating conditions.

Table of Contents

Page

Table of Figures

Page

Table of Tables

0 PREFACE

CHEERS conforms to the European Horizon 2020 Work Programme 2016 – 2017, 10. 'Secure, Clean and Efficient Energy', under the low-carbon energy initiative (*LCE-29-2017: CCS in Industry, including BioCCS)*. The ambition is to improve the efficacy of CO_2 capture in industry, and help ensuring sustainable, secure, and affordable energy.

The action involves a 2nd generation chemical-looping technology tested and verified at laboratory scale (150 kW_{th}). Within the framework of CHEERS, the core technology will be developed into a 3 MW_{th} system prototype for demonstration in an operational environment. This constitutes a major step towards large-scale decarbonisation of industry, offering a considerable potential for retrofitting industrial combustion processes.

The system prototype is based on a fundamentally new fuel-conversion process synthesised from prior research and development actions over more than a decade. The system will include heat recovery steam generation with CO_2 separation and purification, and it will comply with industrial standards, specifications and safety regulations. Except for CO_2 compression work, the innovative concept is capable of removing 96 % of the CO_2 while eliminating capture losses to almost zero.

The CHEERS project is financed by the European Union's Horizon 2020 research and innovation programme under grant agreement No 764697, and co-funded by the Chinese Ministry of Science and Technology (MOST).

0.1 Disclaimer

1 EXECUTIVE SUMMARY

This deliverable, D5.1 CLC reactor-unit modelling, aims at providing the design basis to be considered for the scale-up of the process and the modelling tools to predict the performances of the CLC reactor system. It includes three independent parts :

a) ***Definition of design basis for the industrial unit*** basically provides the application cases that will be considered for the assessment of the CLC technology. A first "Refinery" case consists in the coproduction of steam (500°C, 100 bara) and electricity (50 MWe) to comply with the needs of a typical TOTAL refinery. A second "Power" case considers only production of electricity at a capacity of 200 MWe. A short description of the CLC process is also provided to show the battery limits to be considered for the process simulation and the economical assessment.

b) ***CLC reactor-unit modelling*** presents the development of a turbulent fluidized bed reactor model. Its calibration as well as the equations considered are presented. This model can predict the petcoke conversion accounting for various operating conditions such as temperature, steam content in feeding gas, reactor geometry, oxygen carrier flowrate, petcoke flowrate and properties, etc. It will be further validated using experimental data recorded with the CHEERS demonstration unit.

   The reactor performances predicted with this simulator will be of interest for the industrial scale process cost evaluation accuracy. Indeed, the design of an industrial scale unit will be close to the CHEERS pilot design. Since the software will be validated with CHEERS demonstration unit data, the scale-up ability of the software should be demonstrated. The development of such a model requires knowledge about petcoke gasification kinetics and fluidized bed hydrodynamic modelling. To acquire such knowledge and transpose them to a reactor model, a multi-scale modelling strategy is proposed here.

   First a study in fixed bed and batch bubbling fluidized bed reactor has been undertaken to define and calibrate the petcoke gasification kinetic laws. Then, tests in continuous bubbling fluidized bed reactor are predicted with the model to validate the kinetics determined in batch unit. Finally, new correlations are proposed to account for the change of hydrodynamic in CHEERS demonstration unit and industrial scale units which are operated in turbulent mode instead of bubbling mode.

   In this report, the mechanism of petcoke gasification has been defined with the use of experiments performed in fixed bed reactor. It has been proven experimentally that petcoke is progressively consumed from the inside by water during gasification, which leads to a progressive increase of the petcoke porosity and a decrease of its density over time. The particle radius is assumed to be constant in the model even though a small decrease has been observed experimentally. Carbon dioxide does not seem to impact petcoke gasification rate.

   The comparison between fixed bed and fluidized bed reactor experiments has indicated that petcoke gasification rate is impacted by the oxygen carrier. This impact is linked to the fact that the oxygen carrier oxidizes the produced hydrogen to ensure a constant steam content along reactor height and to a solid/solid interaction between petcoke and oxygen carrier. It was not possible to record independently the solid/solid interaction reaction but to have a more representative reaction rate it was decided to perform the kinetic measurements in the batch fluidized bed reactor. An apparent gasification kinetic is thus considered here.

   Using the kinetic laws calibrated with the batch bubbling fluidized bed reactor, the IFPEN 10 kW pilot plant performances were simulated, and a very good quality of prediction was obtained. These results validate the kinetic laws and parameters proposed.

Finally, using the results of Tom Wytrwat PhD thesis, founded by TOTAL, at Hamburg university, a turbulent hydrodynamic is included in the reactor model to propose a simulation tool representative of the CHEERS demonstration unit and industrial scale unit.

c) ***Characteristics and performance modelling of oxygen carriers*** proposes to develop a thermodynamic screening methodology to identify or rank a set of OCs based on their performance and to provide insights into the suitable operating condition of each OC. This work is a first step in a more exhaustive approach for screening OCs from a thermodynamic and techno-economic perspective.

In this deliverable a framework to find the potential heat recovery from Chemical Looping Combustion (CLC) using different oxygen carriers, based on thermodynamic equilibrium calculations is presented. An equilibrium model based on the minimization of the Gibbs free energy was validated and used to conduct a parametric analysis of the flue gas composition from the CLC fuel reactor using four different oxygen carriers under different process conditions. As an example, the results of the mass and energy balance and potential power production with a simplified CLC process using equilibrium conversions are presented for ilmenite and a nickel-based oxygen carrier.

This framework requires thermodynamic information of the reacting species, which is readily available, and no kinetic information for each oxygen carrier, which is scarcer, is required. As the results of this framework are independent of the configuration of the CLC reactor, this tool can aid in the preliminary evaluation of oxygen carriers with potential for CLC applications and relevant operating conditions.

This framework can be used for the evaluation of different oxygen carriers and can be later refined considering kinetic and design information available within the CHEERS project. In the same fashion, the equilibrium conversion can also be used within a more detailed mass and energy model.

2 PART A: DEFINITION OF DESIGN BASIS FOR THE INDUSTRIAL UNIT

2.1 Application cases

Two application cases have been selected by TOTAL as industrial end-user of the CLC technology.

Case 1 :	**Refinery**
Capacity:	**100 t/h steam (500 °C / 100 bara) and 50 MWe**
Case 2 :	**Power**
Capacity:	**200 MWe**

2.2 Description of CLC plant

The following Block flow diagram describes the CLC plant for the production of electricity and optionally of steam for the refinery case.

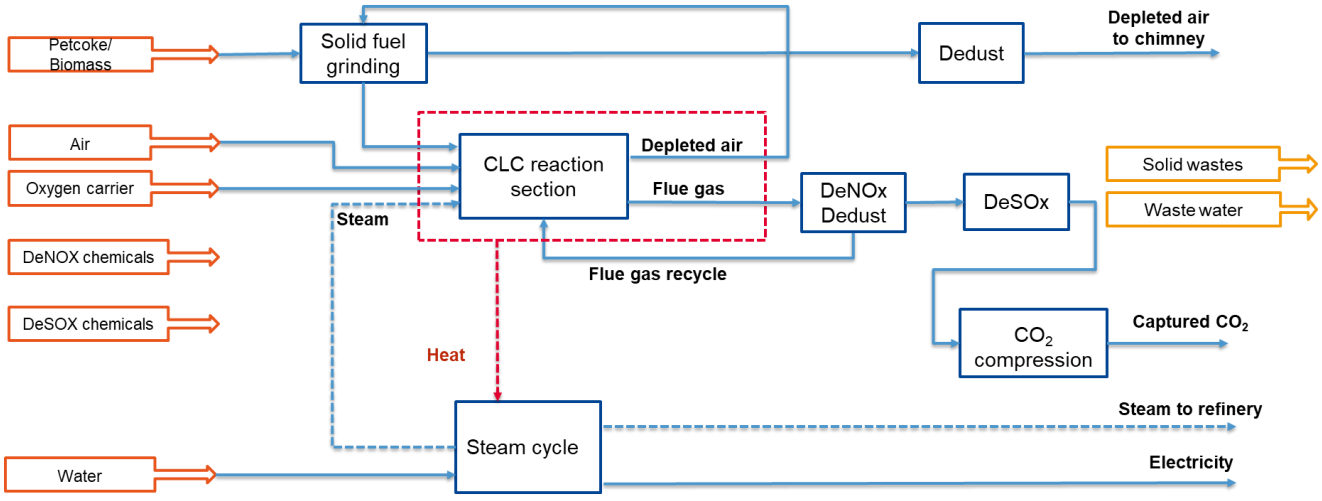

Figure 2-1: Block flow diagram of the CLC process

The CLC reaction section provides heat from the combustion of solid fuel (petcoke or biomass). In contrast to conventional combustion of fuel in the presence of air, CLC involves the use of an oxygen carrier that transfers oxygen from the air to the fuel, preventing direct contact between them. In the CLC system, the oxygen carrier solid is circulated between two reactors, an air and a fuel reactor.

Air is injected in the air reactor and the reoxidation of the oxygen carrier coming from the fuel reactor generates heat, transferred to the solid and to the depleted air exiting the reactor. Depleted air is used to dry the solid fuel during its grinding and is sent to the chimney after a dedust step.

Solid fuel is fed to the fuel reactor, and a mixture of steam and recycled flue gas is injected to fluidize the oxygen carrier particles. By contact with the fluidizing gas, the solid fuel is gasified, and the produced gas is then combusted by contact with the oxygen carrier particles. The flue gas at the outlet of the fuel reactor is mainly composed of CO2 and water, as well as NOx and SOx. The flue gas is therefore treated for deNOx, dedust and deSO_x, prior to the CO2 compression train, in order to meet CO2 specification.

Heat is extracted from the CLC system by exchange with the solid inside the CLC reaction section and with the exhaust gases, i.e. depleted air and flue gas. This heat is transferred to a steam cycle, which converts heat into electricity and can also provide steam to the refinery.

2.3 CO_2 specifications

The following composition is recommended by TOTAL as typical requirement for EOR application.

Table 2-1: Composition of CO_2 product for EOR application

CO_2	%	>95
H_2O	ppmv	500
O_2	ppmv	10
N_2	%	4
Ar	%	4
CH_4	%	4
H_2	%	4
CO	ppmv	35
NOx	ppmv	100
NH_3	ppmv	n.a.
SO_2	ppmv	100
H_2S	ppmv	100
Particles	mg/Nm^3	to be defined by compressor supplier

All general conditions and characteristics of the process are provided in D5.2_a “Common design basis for CCS plant”.

3 PART B: CLC REACTOR-UNIT MODELLING

3.1 A multi scale approach

This strategy allows the development of models which are progressively improved. In this project, four different simulators are developed with a progressive increase of complexity. Each corresponds to one unit involved in the CHEERS project:

- Batch bubbling fluidized bed reactor
  - This small-scale unit operated with 300 g of oxygen carrier is used to select oxygen carrier candidates in Work Package 3. The reactor is filled with an oxygen carrier which is consecutively reduced and oxidized. The fuel used can be methane, hydrogen, carbon monoxide or petcoke (1 g of petcoke injected in the oxygen carrier bed)
  - In Work Package 5, additional experiments have been performed to calibrate the kinetic laws of petcoke gasification.
  - The corresponding model account for bubbling bed hydrodynamic and petcoke gasification kinetics

- Continuous bubbling fluidized bed reactor (10 kw IFPEN unit)
  - Oxygen carrier and petcoke are circulating through the different reactors (fuel and air reactors) composing the unit. The fuel reactor contains around 9 kg of oxygen carrier and the reactors are operated in bubbling bed regimes.
  - The model developed use the kinetic laws and bubbling bed hydrodynamic developed for the batch unit, but the impact of solid circulation is now accounted for.

- The CHEERS demonstration unit
  - It is composed of a continuous turbulent bed coupled with a riser. The experimental results acquired on this unit will be used to validate the model extrapolation to turbulent fluidized bed.
  - The hydrodynamic accounted in the model will be changed from bubbling bed to turbulent bed. A riser model will also be added.

- Industrial scale unit
  - This last simulator developed only requires a change of dimensions with respect to the CHEERS demonstration unit model. Thus, the same simulator is used to simulate both units.

Following these four stages of development, it is therefore possible to provide a simulation tool capable of predicting the performances of an industrial scale unit. In addition to these four units, additional tests have been performed in a fixed bed reactor to improve the understanding of petcoke gasification mechanism and figure out whether kinetics determined in fixed bed are valid in fluidized bed or not.

3.2 Petcoke gasification mechanism

3.2.1 Experimentations in fixed bed reactor

In order to have a better understanding of the mechanism of petcoke gasification, experimentations have been performed in a fixed bed reactor. In this unit, it was possible to perform experiments of petcoke gasification without oxygen carrier. This configuration allows us to avoid petcoke properties modifications due to the grain's friction, which may occur in fluidized bed reactor. Besides, petcoke can be sampled without impurities which allow the recording of petcoke properties evolution more accurately.

3.2.1.1 Unit rig

In Figure 3-1 the fixed bed experimental rig, which is composed of a fixed bed reactor, feeding flow meters and analysers is presented. A sample of devolatilized petcoke is put inside the reactors above a sintered glass and the inlet gas flow, composed of steam and nitrogen, goes through the petcoke bed to gasify it. The carbon dioxide, carbon monoxide and methane profiles are recorded at reactor outlet. To avoid large production of tar in the pilot, devolatilized petcoke is used for this experimentation. This devolatilized petcoke is produced by heating progressively a petcoke sample under nitrogen until a temperature of at least 900 °C.

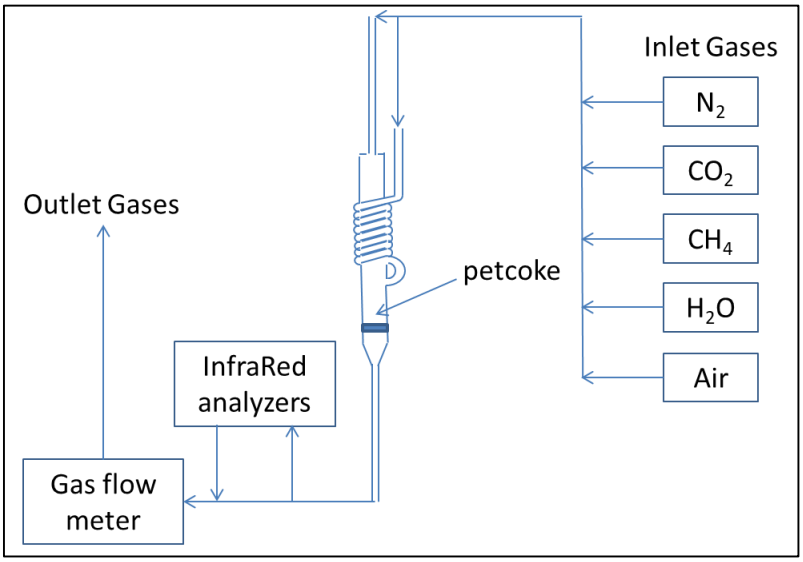

Figure 3-1: Fixed bed unit

3.2.1.2 Experimental procedure

First of all, a complete gasification of petcoke was achieved with 50 mol% of steam at 940 °C. The profile obtained has then been used to correlate the petcoke conversion to the test duration. Then, a series of experiments have been performed in which petcoke gasification was stopped at various time to reach precise petcoke conversion: 10, 20, 50 and 83 %. The petcoke samples retrieved after these tests have been analysed to determine the evolution of petcoke:

- Mean diameter,
- Specific surface,
- Density,
- Porosity.

3.2.1.3 Results

The profiles of carbon monoxide and dioxide measured at reactor outlet during the gasification of petcoke at 940 °C with 50 mol% of steam are presented in Figure 3-2. As presented before, this curve is used to predict the duration of gasification required to reach 10, 20, 50 and 83 % of petcoke conversion. Besides, from these curves, it appears that petcoke gasification shows an activation from 0 to 1500 seconds and then the gasification reaction decreases due to the reduction of the remaining petcoke mass.

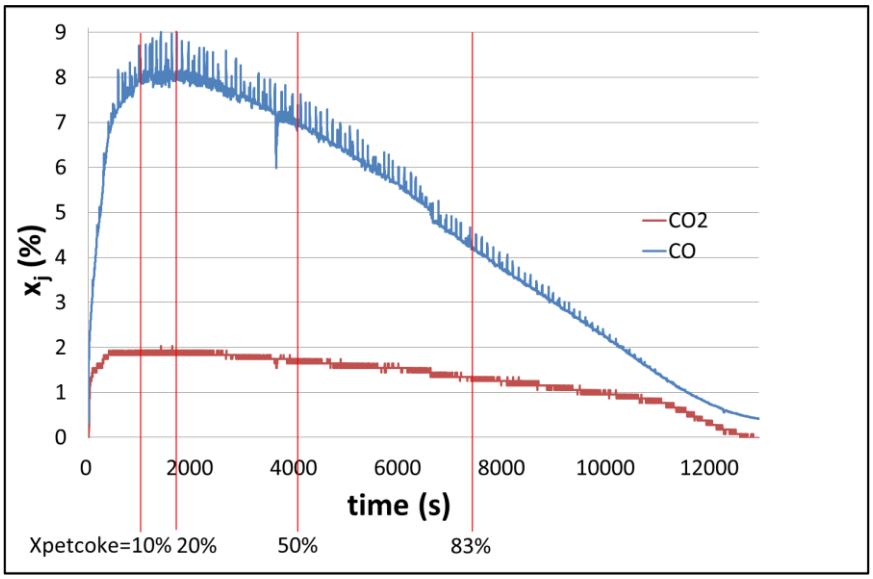

Figure 3-2: Carbon monoxide and dioxide profiles at fixed bed reactor outlet for a gasification with 50 mol% of steam at 940 °C

The evolution of petcoke properties with its conversion is presented in Figure 3-3. Surprisingly, petcoke mean diameter decrease is quite slow. If petcoke was consumed from its surface according to a shrinking core model, the petcoke diameter evolution must respect the following equation 1.

$$D_p = \sqrt[3]{(1 - X_p)\frac{6m_{p,init}}{4\pi\rho}} \qquad 1$$

But the mean diameter decrease does not respect this equation. Since petcoke diameter decrease is slower than expected with a surface consumption mechanism, petcoke must be consumed from the inside and the surface simultaneously.

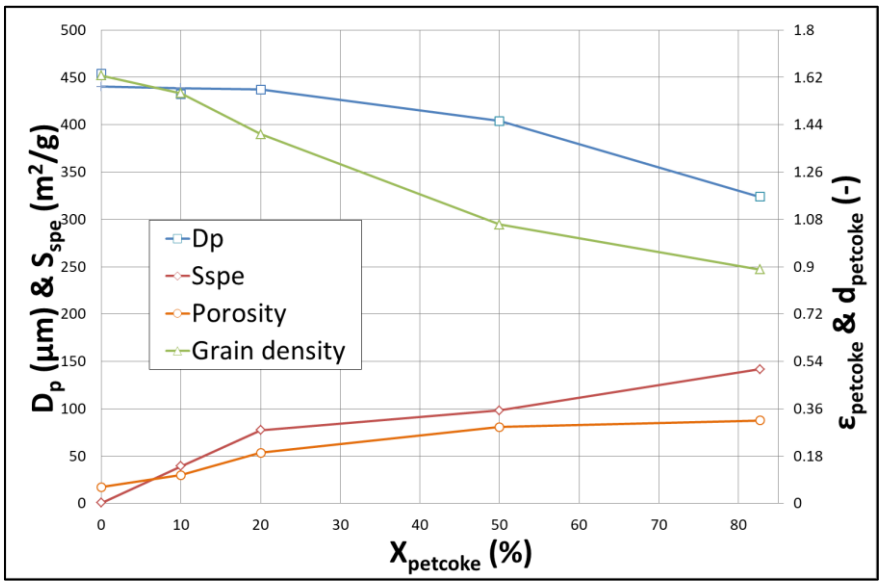

Figure 3-3: Petcoke physical properties evolution in function of its conversion

Petcoke porosity goes from 6 % to around 30 % and its specific gravity decreases from 1.62 to 0.9. Thus, it confirms the hypothesis of a petcoke consumption from the inside by steam which open petcoke porosity leading to the observed increase in specific surface S_{spe} (from close to 0 to 140 m^2/g). Numerically, the gasification kinetics used in IFPEN model account for the specific surface modifications, as well as the density decrease, but the grain mean diameter is supposed to be unchanged to reduce the model complexity and improve its stability. The grain representation is presented in Figure 3-4.

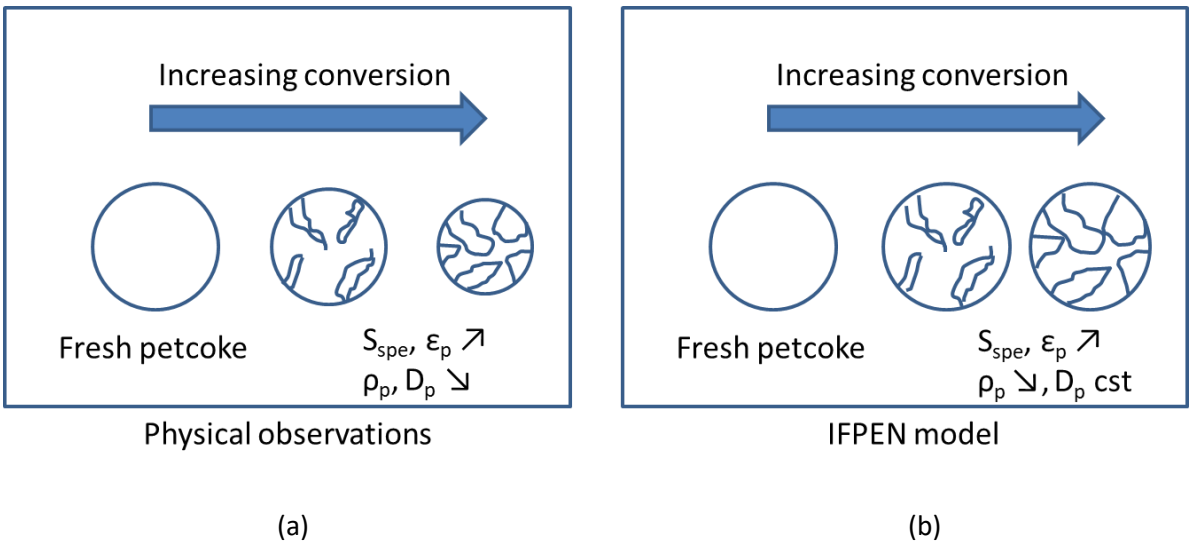

Figure 3-4: Petcoke properties evolution (a) based on physical measurement and (b) accounted for in the IFPEN model

3.2.2 Experimentation in batch fluidized bed reactor

In order to determine whether kinetic experiments should be conducted in fixed bed reactor or fluidized bed reactor to correctly measure petcoke gasification reaction, a comparative study has been undertaken with experimental results acquired in both units.

3.2.2.1 Unit rig

The batch fluidized bed unit used for the petcoke gasification kinetic study is presented in Figure 3-5.

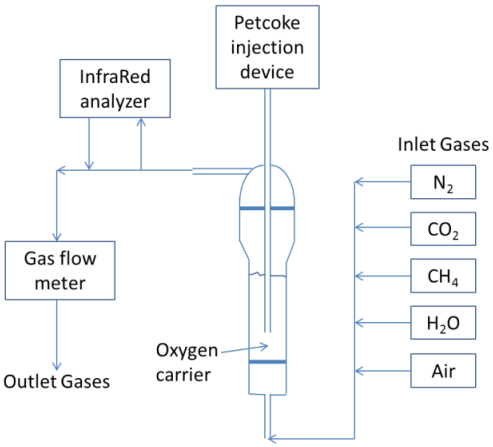

Figure 3-5: Batch fluidized bed unit

This unit is composed of:

- various gas feeders to inject a gas mixture composed of CH_4, H_2O, N_2, Air and/or CO_2 in the reactor,
- a reactor which can be used for gaseous and solid fuel tests,
- an outlet gas analyzer to determine the outlet gas phase composition,
- a gas flow meter.

The oxygen carrier is not moving out of the reactor. Thus, material reduction/oxidation cycles are performed by changing the reactor inlet gas phase composition.

3.2.2.2 Experimental procedure

For safety reason, for gaseous fuels, a reduction/oxidation cycle is decomposed of four stages with different feeding gas compositions:

- inerting step: N_2
- reduction step: CH_4/CO_2
- inerting step: N_2
- oxidation step: Air

The material reduction degree is adjusted by changing the reduction step duration (time during which methane mixture is injected). Full oxidation of the oxygen carrier is always ensured by adaptation of the oxidation step duration.

For petcoke tests the following steps are considered:

- inerting step: N_2/H_2O
- reduction step: petcoke injection in the oxygen carrier bed with unchanged N_2/H_2O mixture
- oxidation step: Air

Here, an atmosphere rich in steam is going through the reactor during the inerting step. Petcoke is injected in the reactor without changing the gas phase composition. After the petcoke injection, the Reduction step duration is adjusted to ensure a chosen petcoke conversion. Then the feeding gas is switched to air to burn the remaining petcoke and oxidize the oxygen carrier.

In order to avoid solid plugging in the petcoke feeding tube, 40 NL/h of nitrogen is always injected through this tube during tests.

The oxygen carrier considered to develop this model is an Ilmenite from Titania selected in Work Package 3 of the CHEERS project. This material requires several cycles of reduction/oxidation to stabilize its reactivity. Thus, 50 cycles with methane as fuel are performed before injecting petcoke in the reactor. The operating conditions of this pre-ageing test are:

- Height of the fluidized oxygen carrier ~ 12 cm (~ 300 g for ilmenite materials),
- Total gas flow rate = 190 NL/h
- Temperature = 900°C
- Petcoke feeding tube flowrate = 40 NL/h of N_2
- Gaseous fuel gas composition = 50 % CH_4/ 50 % CO_2

When material reactivity is stabilized. Several injections of 1 g of petcoke are undertaken with various operating conditions listed in Table 3-1 following the procedure presented above.

Table 3-1: List of operating condition

Test n°	T	Petcoke Mean Diameter	Oxygen carrier mass	Petcoke injected mass	Total gas flowrate	Fluidization gas composition			Aim of the test
						xN_2	xH_2O	xCO_2	
	°C	µm	g	g	NL/h	mol%	mol%	mol%	
1	940	270	290	1	184	50	50	0	reference
2	940	270	290	1	184	21	**16**	**63**	Impact CO_2 and H_2O
3					184	21	**32**	**47**	
4					184	21	**50**	**29**	
5					193	20	**64**	**16**	
6	**850**	270	290	1	198	21	50	29	Impact of temperature
7	**900**				190				
8	940	**157**	290	1	193	20	64	16	Impact of petcoke size
9					184	21	50	29	
10	900				190				

Among the tests performed, some of them were done with a petcoke with a smaller mean diameter. The aim of these tests is to check if the particle diameter impacts the petcoke reactivity. Indeed, if the reaction does not depend on petcoke surface but only on petcoke volume, petcoke size should not impact the gasification rate.

In order to compare petcoke reactivity in fluidized bed and in fixed bed reactors, tests have also been performed with inert sand instead of the oxygen carrier in fluidized bed reactor.

3.2.2.3 Comparison between experimental tools

It was possible to perform experiments in fixed bed and fluidized bed reactors with similar operating conditions (gas flowrate, steam content, petcoke mass and temperature). The main differences lie in:

- The 300 g of inert sand used in fluidized bed reactors to have a bed hydrodynamic representative of a real test with oxygen carrier.
- The gas flow going upward in fluidized bed and downward in fixed bed.

Devolatilized petcoke has been used for both experiments.

Using the two units available, tests have been performed to:

- Compare a fixed bed and a fluidized bed (operated with sand) using devolatilized petcoke,
- Determine the impact of petcoke devolatilisation in fluidized bed reactor with sand,
- Study the use of sand or an oxygen carrier in fluidized bed reactor.

This study has been performed with two petcokes as presented in Figure 3-6. The first petcoke was provided by TOTAL and is the reference petcoke used for oxygen carrier screening in Work package 3. The second petcoke is the one with low sulphur content selected for the CHEERS project.

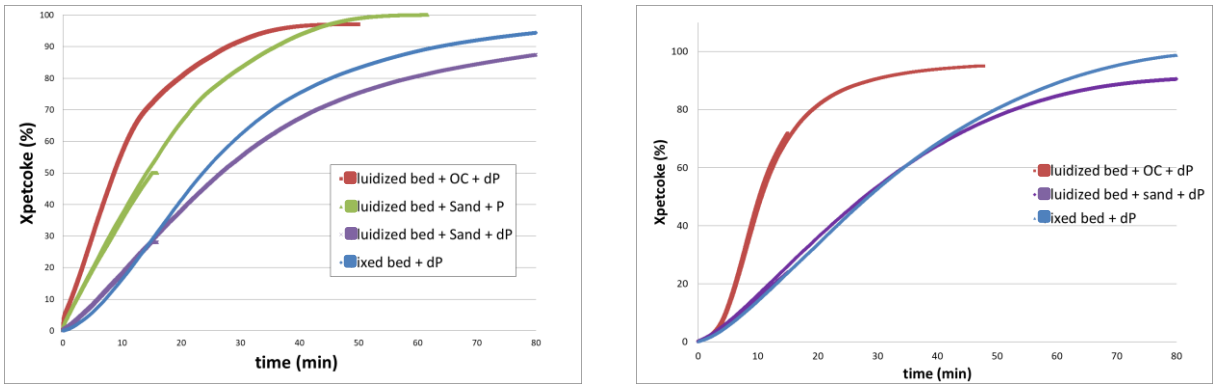

(a) (b)

Figure 3-6: Comparison of devolatilized petcoke conversion evolution with time in (red) fluidized bed reactor with oxygen carrier, (purple) fluidized bed reactor with sand and (blue) fixed bed reactor at 940 °C with 50 mol% of steam. Evolution of non-devolatilized petcoke conversion with time in (green) fluidized bed reactor with sand. Study made with a petcoke from (a) TOTAL and (b) Chinese partners.

In this Figure 3-6, the comparison of the blue curves obtained in fixed bed and the purple curves corresponding to a fluidized bed reactor operated with sand indicates that the petcoke gasification rate is not significantly different in both units. Consequently, the friction encountered in fluidized bed reactors does not impact petcoke gasification rate and kinetics measured in fixed bed reactor are still valid in fluidized bed reactor with an inert bed.

The comparison of purple and red curves in Figure 3-6Figure 3-6 (a) and (b) indicates that petcoke gasification is greatly impacted by the presence of oxygen carrier. This impact can come from:

- the boost of reactivity brought by the reoxidation of hydrogen in water maintaining a high steam concentration
- direct reaction between petcoke and the oxygen carrier.

Using the model presented in this report, it has been confirmed that the reoxidation of hydrogen alone is not able to explain this reactivity gain. Consequently, there is an interaction between petcoke and the oxygen carrier, which is not measured in fixed bed reactors.

Finally, the comparison of green and blue curves in Figure 3-6 (a) indicates that the methods of volatiles removal impact greatly the petcoke gasification kinetics. Indeed, when petcoke is devolatilized beforehand, the volatiles are removed by a smooth heating of the petcoke from ambient to 900 °C at 10°C/min. For tests with non-devolatilized petcoke, the petcoke sample injected directly in the fluidized bed is heated from ambient to 900 °C in a few seconds. The fast release of the volatiles may favour the porosity opening of the petcoke grains which improves greatly the petcoke gasification rate with respect to tests with devolatilized petcoke.

As a consequence, all kinetics measured with a petcoke heated smoothly drive to an underestimation of the real process performances. That is why IFPEN has undertaken experiments in the batch fluidized bed reactor to calibrate the model.

Finally, it is not possible to fully understand the mechanism of interaction between petcoke and oxygen carrier with the current data base. Thus, a global kinetic of petcoke gasification has been calibrated using the results obtained in this batch fluidized bed reactor using ilmenite as oxygen carrier. This oxygen carrier being currently the one selected for the CHEERS demonstration unit operation.

3.2.2.4 Kinetic results

In Figure 3-7Figure 3-7 typical results obtained in the batch unit are presented.

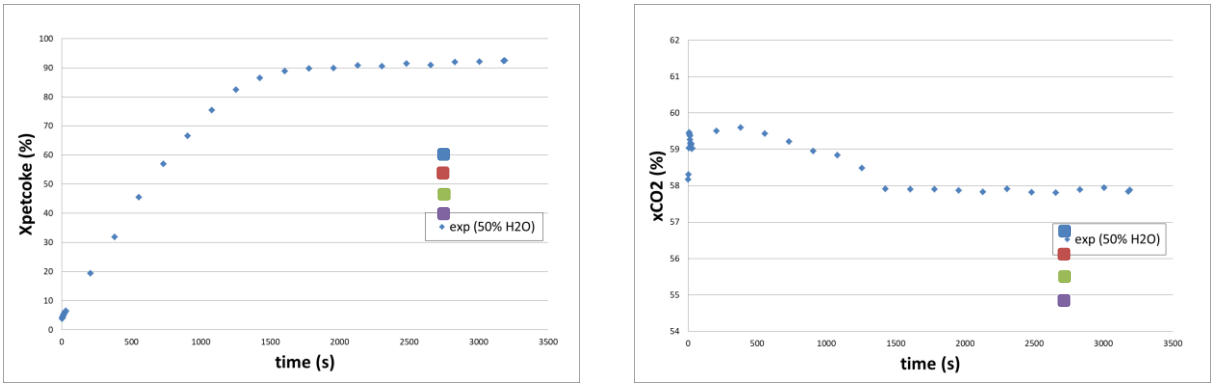

(a) (b)

*Figure 3-7: Evolution of (a) Xpetcoke and (b) carbon dioxide outlet concentration with time for the reference steam concentration (50 mol% **diluted in CO_2**) at 940 °C*

From all the experimentation performed the following conclusions have been made:

- Petcoke reactivity shows an activation in fixed bed and in fluidized bed reactor,
  - In the model, this behaviour will be predicted using the petcoke properties evolution measured in fixed bed reactor (specific surface, density, etc.)
- Carbon dioxide does not impact petcoke gasification rate,
- Steam and temperature are the main operating conditions impacting petcoke reactivity,
- For steam content above 50 mol% the gain in reactivity is limited,
- Petcoke size has a limited effect on petcoke reactivity,
  - The grain representation proposed in part 3.2.1.3 will be used in the model.

3.3 Batch bubbling fluidized bed reactor model

3.3.1 Two phases approach

To model the hydrodynamic of a bubbling fluidized bed reactor, a two phases approach has been selected as presented in Figure 3-8. This type of multiphasic models has been developed by Toomy and Johnstone [1] and Davidson and Harrison [2] and improved by Wen and Fan [3]. It is generally used to have a better representation of the bed hydrodynamic and account for various physical phenomena. Two phases are considered in this model:

- The bubble phase
- The dense phase

All the solid particles are in the dense phase. Bubbles, composed of gas only, go up through the bed with an increasing size. The hold-up of gas in the bubble and dense phases and the solid hold-up are defined as the volume of gas in bubble and dense phase and the volume of solid over the reactor volume.

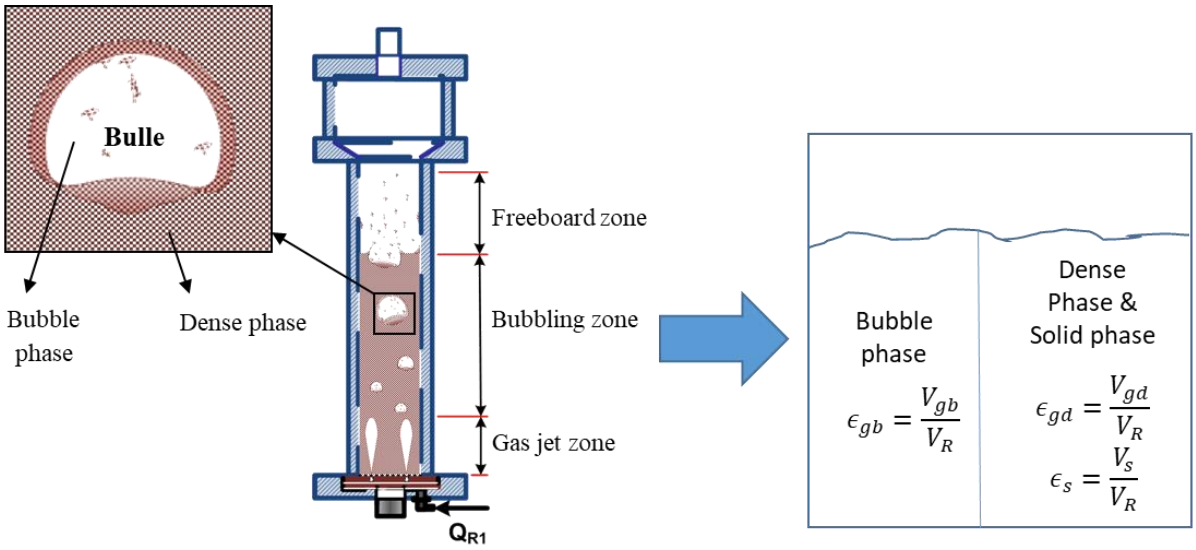

Figure 3-8: Bubbling fluidized bed two phases representation

In this model, the bed is divided in layers and hydrodynamic correlations are used to calculate the hold-ups axial evolution and mass transfer between the phases. Mass balances are solved to predict each element concentration for all layers. To avoid any numerical stiffness in the model, the gas and solids hold-ups are initialized before solving the mass balances and not changed again during the time integration. The variations of the flow of gases produced by petcoke conversion will impact the bubbles velocity without changing the gas hold-ups.

3.3.2 Mass balances

The variation of the concentrations of gaseous compounds in bubble and dense phases are represented by the following mass balances:

$$S.\varepsilon_{gb}\frac{\partial C^{i}_{gb}}{\partial t} = -\frac{\partial (S.V_{sgb}.C^{i}_{gb})}{\partial z} - K_{bd}.S.\varepsilon_{gb}(C^{i}_{gb} - C^{i}_{gd}) + \frac{Q_t C^{i}_{gd}}{dz} \qquad 2$$

$$S.\varepsilon_{gd}\frac{\partial C^{i}_{gd}}{\partial t} = D_{ax,g}\frac{\partial (S.\varepsilon_{gd}.\partial C^{i}_{gd}/\partial z)}{\partial z} - \frac{\partial (V_{sgd}.S.C^{i}_{gd})}{\partial z} + K_{bd}.S.\varepsilon_{gb}(C^{i}_{gb} - C^{i}_{gd}) + S.\rho_S.\varepsilon_S\sum_j \mu_{ij}.r_j - \frac{Q_t.C^{i}_{gd}}{dz} \qquad 3$$

With:

S: reactor section (m²),
ϵ_{gb}: bubble phase gas hold-up (m³/m³),
C^{i}_{gb} : concentration of gaseous component *i* in bubble phase (mol/m³),
t : time (s),
z : reactor abscissa (m),
$V_{sg,b}$: superficial gas velocity in bubble phase (m/s),
K_{bd}: mass transfer coefficient between bubble and dense phase (m/s),
Q_t : volumetric flow transferred between bubble and dense phases (m³/s),
ϵ_{gd}: dense phase gas hold-up (m³/m³),
C^{i}_{gd} : concentration of gaseous component *i* in dense phase (mol/m³),
$D_{ax,g}$: dense gas phase axial dispersion coefficient (m²/s)
$V_{sg,d}$: superficial gas velocity in dense phase (m/s),
ρ_S: solid specific gravity (petcoke or oxygen carrier) (kg/m³),
ϵ_S: solid phase hold-up (petcoke or oxygen carrier) (m³/m³),
μ_{ij}: stoichiometric coefficient of reaction *j* for component *i* (-),
r_j: reaction *j* rate (mol/m³/s)

These equations account for:

- Gas convection through the bed,
- Mass transfer due to a difference of components concentration in bubble and dense gas phases,
- Volumetric mass transfer of gas between gas phases due to the production or consumption of gas by the reaction in dense phase. Indeed, in this model, the gas superficial velocity in dense phase is defined by the hydrodynamic calculations presented in part 3.3.3.4 . In order to maintain the dense phase gas velocity at the calculated value and account for the variations of the amount of gas produced by the reactions, a gas flow is transferred between bubble and dense phases.
- Gas axial dispersion in dense phase,
- Reactions between gaseous components and the oxygen carrier and petcoke.

The axial gas dispersion coefficient ($D_{ax,g}$) and the mass transfer coefficient between bubble and dense phase (K_{be}) are given by correlations presented in the hydrodynamic section (part 3.3.3). The volumetric flow transferred between bubble and dense phases is given by a combination of mass balance equations (equation 4) and is calculated at each time step during the mass balances integration.

$$Q_t = \frac{dz}{R_g \sum C_{gd}^i}\left(D_{ax,g}.\frac{\partial}{\partial z}\left(S.\varepsilon_{gd}.\frac{\partial(P_z/T)}{\partial z}\right) - \frac{\partial}{\partial z}\left(V_{sg,d}.S.\frac{P_z}{T}\right) + \sum_i S.R_g.K_{bd}.\varepsilon_{gb}.\left(C_{gb}^i - C_{gd}^i\right) + R_g.S.\rho_s.\varepsilon_s.\sum_i\sum_j \mu_{ij} r_j\right) \quad (4)$$

With:

P_z: pressure in the layer z (Pa),
R_g: ideal gas constant (J/mol/K),
i: component number (-),
j: reaction number (-)

In order to account for the amount of gas produced by the reaction of petcoke gasification and the oxygen carrier reactions, the total gas superficial velocity V_{sg} is integrated as well over time. The time derivate of the total superficial gas velocity is given in equation 5.

$$\frac{\partial}{\partial z}\left(V_{sg}.S.\frac{P_z}{T}\right) = D_{ax,g}.\frac{\partial}{\partial z}\left(S.\varepsilon_{gd}.\frac{\partial}{\partial z}\left(\frac{P_z}{T}\right)\right) + R_g.S.\sum_i\sum_j \mu_{ij}\rho_s r_j \varepsilon_s \quad (5)$$

With:

V_{sg}: total superficial gas velocity in reactor (m/s),

The dense phase gas superficial velocity is calculated by a correlation presented in hydrodynamic section (part 3.3.3.4). The remaining gas flow goes to the bubble phase.

Finally, the evolution of solid components concentration evolution is given by the following equation 6.

$$S.\varepsilon_s.\frac{\partial C_S^i}{\partial t} = D_{ax,s}\frac{\partial\left(\varepsilon_S.S.\partial C_S^i/\partial z\right)}{\partial z} + \rho_s.S.\varepsilon_s\sum_j \mu_{i,j}.r_j \quad (6)$$

With:

C_S^i : concentration of component i in solid phase (mol/m³),

These equations are integrated over time to predict the evolution of gas and solid compounds concentration and gas velocity. The hold-ups and the pressure drop are initialized before the integration of these equations and stay unchanged over time to reduce the model stiffness. When more gas goes in the bubble phase, the hold-up will stay unchanged and the bubble gas superficial and real velocities will be impacted. It corresponds to bubbles with a global volume but showing variation of velocity.

3.3.3 Bubbling bed hydrodynamic

In this part the axial dispersion coefficient, mass transfer coefficient between bubble and dense phases, and hold-ups and pressure drop calculations are presented.

3.3.3.1 Axial dispersion coefficients

The dense gas phase axial dispersion coefficient ($D_{ax,g}$) is given by equation 7 according to Kunii and Levenspiel [4]

$$D_{ax,g} = 0.3{D_R}^{0.65} \quad (7)$$

With:

D_R : the reactor diameter (m)

And the solid phase axial dispersion coefficient ($D_{ax,s}$) is calculated from equation 8 with a peclet Pe_S equal to 5 determined experimentally with IFPEN pilot (internal report R1230S-TS/IS-n°13-0419).

$$D_{ax,s} = \frac{u_{gd} H_{bed}}{Pe_S} \quad (8)$$

With:

u_{gd}: dense phase gas real velocity (m/s),
H_{bed} : bed height (m),

3.3.3.2 Mass transfer coefficient between bubble and dense phase

Kunii and Levenspiel [5] proposed the following correlations presented in equations 9, 10 and 11 to calculate this coefficient. This mass transfer coefficient between bubble and dense phases account for a cloud phase located between dense and bubble phases. In IFPEN model, only the global mass transfer coefficient between bubble and dense phases (K_{bd}) is used.

$$K_{bd} = \frac{1}{\frac{1}{K_{bc}} + \frac{1}{K_{cd}}} \quad (9)$$

With:

K_{bc}: mass transfer coefficient between bubble and cloud (m/s)
K_{cd}: mass transfer coefficient between cloud and dense phase (m/s)

$$K_{bc} = 4.50\left(\frac{U_{mf,OC}}{d_b}\right) + 5.85\left(\frac{{D_m}^{0.5} g^{\frac{1}{4}}}{{d_b}^{\frac{5}{4}}}\right) \quad (10)$$

With:

d_b : bubble diameter (m),
D_m: gas molecular diffusivity (m²/s),
g: earth gravity (m/s²)
$U_{mf,OC}$: oxygen carrier minimal fluidization velocity (m/s)

$$K_{cd} = 6.77\left(\frac{D_m 0.711\sqrt{g d_b}}{d_b^3}\right)^{\frac{1}{2}} \quad 11$$

The bubble diameter at a height *h* in the reactor is given by equation 12 presented in the work of Werther [6].

$$d_b = 8.53\times10^{-3}\sqrt[3]{1+27.2(V_{sg}-U_{mf,OC})}(1+6.48h)^{1.21} \quad 12$$

With:

h: height position in the bed (m),

3.3.3.3 Minimal fluidization velocity

The particles minimal fluidization velocity is given by equations 13 and 14 from [7]

$$Re_{mf} = \sqrt{27.2^2 + 0.0408Ar} - 27.2 = \frac{\rho_g d_p U_{mf,OC}}{\mu_g} \quad 13$$

$$Ar = \frac{g.d_p^3 \rho_g (\rho_s - \rho_{OC})}{\mu_g^2} \quad 14$$

With:

d_p: particle diameter (m)
ρ_g: gas specific gravity (kg/m^3)
μ_g: gas viscosity (Pa.s)

3.3.3.4 Gas superficial velocity calculation

The gas superficial velocity is the total gas flow rate going through the reactor divided by the reactor section. The gas repartition is divided between bubble and dense phases. For the bubbling bed model, it is assumed that the dense phase gas superficial velocity is equal to the oxygen carrier minimal fluidization velocity, so that the solid fluidization is ensured. All the remaining gas goes in the bubble phase as it is presented in equations 15 and 16.

$$V_{sg,d} = U_{mf,OC} \quad 15$$

$$V_{sg,b} = V_{sg} - V_{sg,d} \quad 16$$

3.3.3.5 Hold-ups calculation

The gas and solid phases hold-ups are calculated following this methodology:

- Calculation of the axial dispersion coefficients (correlations part 3.3.3.1)
- Calculation of the mass transfer coefficient between bubble and dense phase (correlations part 3.3.3.2)
- Calculation of the gas total superficial velocity (equation 5 part 3.3.2)
- Calculation of gas superficial velocity in dense and bubble phases (equations part 3.3.3.4)
- Calculation of the minimal fluidization velocity (correlations part 3.3.3.3)
- Calculation of the bubble velocity given by equation 17

$$u_{gb} = V_{sg,b} + 0.711\sqrt{g.d_b} \quad (17)$$

- Calculation of gas and solid hold-up with equations 18, 19, 20 and 21.

$$\epsilon_{gb} = \frac{V_{sg,b}}{u_{gb}} \quad (18)$$

$$\epsilon_{gd} = (1 - \epsilon_{gb})\epsilon_{mf} \quad (19)$$

$$\epsilon_{OC} = (1 - \epsilon_{gb} - \epsilon_{gb})\frac{m_{OC}}{m_{OC} + m_P} \quad (20)$$

$$\epsilon_P = (1 - \epsilon_{gb} - \epsilon_{gb})\frac{m_P}{m_{OC} + m_P} \quad (21)$$

With:

ϵ_P: petcoke hold-up (m^3/m^3)
ϵ_{OC}: oxygen carrier hold-up (m^3/m^3)
ϵ_{mf}: gas holdup at the minimal fluidization velocity (m^3/m^3)
m_P : mass of petcoke injected in the reactor (kg)
m_{OC} : oxygen carrier mass in the reactor (kg)

The ratio of petcoke volume over oxygen carrier volume is supposed constant since it is assumed that petcoke particle volume is not impacted by its conversion (cf part 3.2.1.3) as well as the oxygen carrier volume. These hold-ups are initialized at the beginning of a simulation and are not changed later on. Tests have been performed before hand to ensure a good distribution of the petcoke in the oxygen carrier bed. An initial homogeneous petcoke distribution is supposed in the model.

3.3.3.6 Bed pressure drop

The bed pressure drop is calculated when solid hold-ups are known with the following equation 22. Assuming bed is divided in layers, the pressure at a bed axial position P_{z-1} is equal to the pressure at the layer above P_z plus the oxygen carrier weight. Petcoke weight is neglected here.

$$P_{z-1} = P_z + \rho_{OC} g \epsilon_{OC} dz \quad (22)$$

With:

dz : bed layer thickness (m)

3.3.4 Reaction scheme and kinetic laws

The model is calibrated considering a Chinese petcoke with a low sulphur content and an ilmenite oxygen carrier. The petcoke volatiles nature and amount have been estimated using the petcoke CHONS composition before and after devolatilization. The global reactions of petcoke gasification are:

Petcoke → Volatiles + Char

Char + steam → gasified products + Ash

The elemental composition of Petcoke, Volatiles, Char and Ash is presented in Table 3-2. Ash is supposed to be SiO_2.

Table 3-2: molar composition of Petcoke, Volatiles, Char and Ash

	C	H	O	N	S	Si
Petcoke	0.6331	0.3410	0.0089	0.0150	0.0013	0.0007
Volatiles	0.0703	0.8853	0.0196	0.0248	0	0
Char	0.8825	0.0999	0.0041	0.0106	0.0019	0.0010
Ash	0	0	2	0	0	1

Based on experimental results and these elements composition the following reaction scheme has been defined to represent petcoke gasification

$$\text{Petcoke} \rightarrow 0.299\ \text{Volatiles} + 0.701\ \text{Char} \qquad \text{r0}$$

$$\text{Volatiles} \rightarrow 0.051\ CH_4 + 0.341\ H_2 + 0.020\ CO + 0.012\ N_2 \qquad \text{r1}$$

$$\text{Char} + 0.895\ H_2O \rightarrow 0.001\ \text{Ash} + 0.945\ H_2 + 0.882\ CO + 0.011\ NO + 0.002\ SO_2 \qquad \text{r2}$$

r0 is assumed to be an instantaneous reaction of petcoke dissociation in volatiles species and char. Then, the very fast reaction of volatiles release (r1) occurs. Knowing the Volatiles composition, it is decomposed in CH_4, H_2, CO and N_2 to respect the mass balance. In this model, it is assumed that the nitrogen contained in biomass is released as approximately two third of NO and one third of N_2 while the sulphur is 100 % released as SO_2. Unfortunately, the measurements of NOx and SOx species in the batch unit were not accurate enough to confirm with these hypotheses. It will be possible to have more accurate data from the CHEERS demonstration unit and improve the current model.

The very fast reaction rate of volatiles release (r1) is defined as:

$$r_{Vol} = k_1^0 e^{-\frac{E_{a,1}}{RT}} C_{Vol} \qquad 23$$

With:

k_1^0 : pre-exponential constant of reaction 1 ($m^3/kg/s$)
$E_{a,1}$: Activation energy of reaction 1 (J/mol)
C_{Vol} : Volatiles concentration in petcoke (mol/m^3)

For char gasification (r2), the following reaction rate has been selected.

$$r_{Char} = k_2^0 e^{-\frac{E_{a,2}}{RT}} C_{H_2O,gd}^n C_{Char}^m S_{spe} (X_p)^o \qquad 24$$

With:

k_2^0 : pre-exponential constant of reaction 2 (SI)
$E_{a,2}$: Activation energy of reaction 2 (J/mol)
C_{Char} : Char concentration in petcoke (mol/m^3)
$C_{H_2O,gd}$: Water concentration in dense gas phase (mol/m^3)

S_{spe} : Petcoke specific surface (m^2/kg)
X_p : Petcoke conversion (-)
n, m, o: reaction orders (-)

In this kinetic law, the impact of petcoke specific surface evolution is accounted for through a power function term.

Methane, hydrogen and carbon monoxide oxidation by ilmenite are not limiting reactions in this process. Nevertheless, ilmenite reactivity is represented by the following reaction scheme.

$CH_4 + 3\ Fe_2O_3 \rightarrow 2\ Fe_3O_4 + CO + 2\ H_2$ r3

$CH_4 + Fe_3O_4 \rightarrow 3\ FeO + CO + 2\ H_2$ r4

$CO + 3\ Fe_2O_3 \rightarrow 2\ Fe_3O_4 + CO_2$ r5

$CO + Fe_3O_4 \rightarrow 3\ FeO + CO_2$ r6

$H_2 + 3\ Fe_2O_3 \rightarrow 2\ Fe_3O_4 + H_2O$ r7

$H_2 + Fe_3O_4 \rightarrow 3\ FeO + H_2O$ r8

All these reactions are considered to following a shrinking core mechanism with the following kinetic laws applicable for CH_4 (equation 25), CO (equation 26) and H_2 (equation 27).

$$r_{3\ and\ 4,j} = \frac{3C_{CH4,gd}^{n} C_{OC}^{m}}{\frac{R_p^2\left(1-(1-X_{OC})^{1/3}\right)}{D_{e,j}^{0} e^{-\frac{E_{a,De,j}}{RT}}(1-X_{OC})^{2/3}} + \frac{R_p}{k_j^0 e^{-\frac{E_{a,j}}{RT}}(1-X_{OC})^{2/3}}} \quad 25$$

$$r_{5\ and\ 6,j} = \frac{3C_{CO,gd}^{n}}{\frac{R_p^2\left(1-(1-X_{OC})^{1/3}\right)}{D_{e,j}^{0} e^{-\frac{E_{a,De,j}}{RT}}(1-X_{OC})^{2/3}} + \frac{R_p}{k_j^0 e^{-\frac{E_{a,j}}{RT}}(1-X_{OC})^{2/3}}} \quad 26$$

$$r_{7\ and\ 8,j} = \frac{3C_{H2,gd}^{n}}{\frac{R_p^2\left(1-(1-X_{OC})^{1/3}\right)}{D_{e,j}^{0} e^{-\frac{E_{a,De,j}}{RT}}(1-X_{OC})^{2/3}} + \frac{R_p}{k_j^0 e^{-\frac{E_{a,j}}{RT}}(1-X_{OC})^{2/3}}} \quad 27$$

With:

C_{OC} : oxygen carrier reactant (Fe_2O_3 or Fe_3O_4) concentration (mol/m^3)
X_{OC}: oxygen carrier conversion (-)
R_p: Oxygen carrier particle radius (m)
$D_{e,j}^{0}$: pre-exponential factor of reaction j effective diffusion coefficient (m^2/s)
$E_{a,De,j}$: activation energy of the effective diffusion coefficient (J/mol)

All the kinetic parameters are calibrated with tests performed in the batch fluidized bed reactor. For ilmenite reactivity towards methane, dedicated tests have been performed. The reactivity of carbon monoxide and hydrogen with ilmenite are too high to be correctly recorded in IFPEN pilot. Thus, the kinetic parameters proposed here have been set to predict a full conversion of CO and H_2 in the IFPEN pilot but their accuracy is limited.

3.3.5 Model calibration

First of all, ilmenite reduction kinetics have been adjusted using experiments performed with methane as fuel. Carbon monoxide and hydrogen oxidation by ilmenite are too fast to be correctly calibrated. Nevertheless, methane conversion has been precisely adjusted to predict the experiments presented in Figure 3-9. The small deviation at the beginning of the test corresponds to a time delay due to the analytical response time.

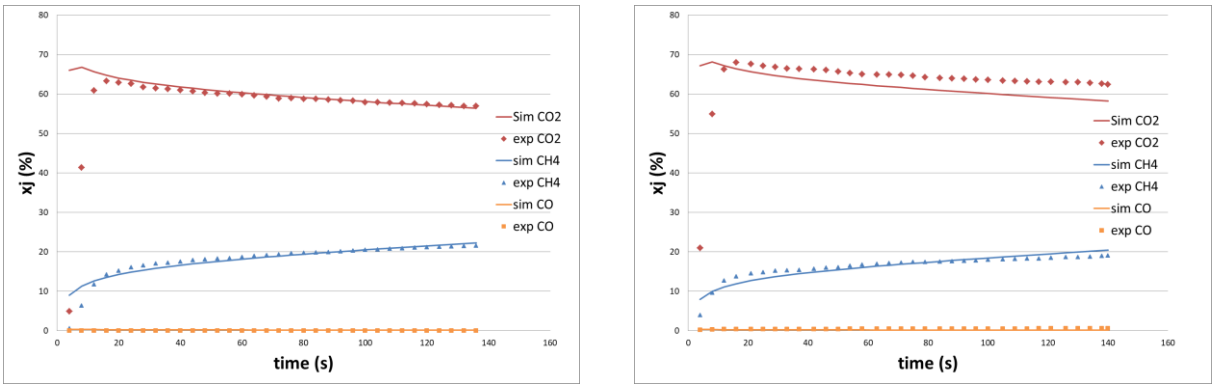

Figure 3-9: Evolution of methane conversion over time at (left) 900 °C and (right) 940 °C.

In order to determine the impact of carbon dioxide on petcoke gasification kinetics, two tests have been performed with similar operating conditions : 50 % of steam, 940°C, same gas flowrate, same oxygen carrier and petcoke mass but with a different carbon dioxide concentration (0 % and 29 %). Nitrogen is used as diluting gas. As it is visible in Figure 3-10 the presence of carbon dioxide does not impact the petcoke conversion. Besides, the model proposed here is able to predict the activation of petcoke observed experimentally.

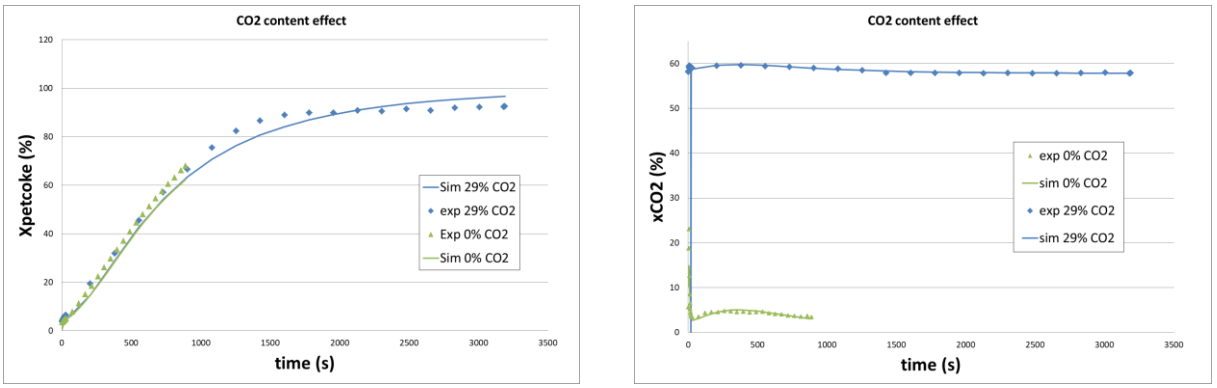

Figure 3-10: Evolution of (left) petcoke conversion and (right) carbon dioxide profiles over time at 940 °C with 50 mol% of steam diluted with 29 % or 0 % of carbon dioxide. The remaining fraction is nitrogen

The model prediction is quite good for the whole range of operating conditions, from 850 to 940 °C and from 16 % to 64 % of steam content. This model does not account for the impact of petcoke diameter. But the tests performed with smaller petcoke size (mean diameter of 157 µm instead of 270 µm) are well predicted until a petcoke conversion of 80 %. For higher conversion, the model seems to over-predict petcoke conversion. Nevertheless, accounting for the experimental accuracy, the kinetic model is assumed to be validated.

The hydrodynamic part of the model proposed here will be updated to simulate experiments performed in IFPEN 10 kWth CLC pilot using the same kinetic laws.

3.4 Continuous bubbling fluidized bed reactor model

3.4.1 Experimental rig

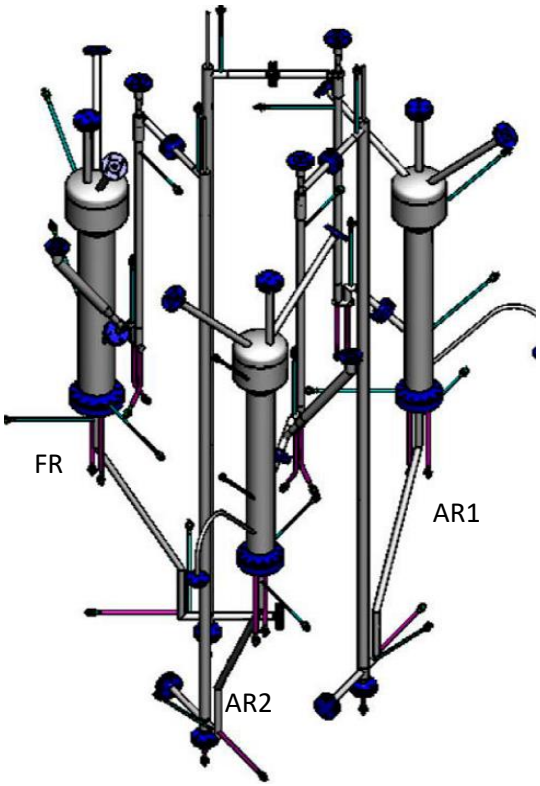

Figure 3-11: 3D scheme of the pilot plant

A schematic view of IFPEN's 10 kW_{th} CLC pilot unit used in this study is shown in Figure 3-11. The pilot is composed of three interconnected bubbling fluidized bed reactors and a carbon stripper. Two fluidized bed reactors (AR1 and AR2) are dedicated to the oxygen carrier oxidation and the third one (FR) is dedicated to fuel combustion, therefore performing OC reduction. In the fuel reactor, gaseous fuel or petcoke can be injected to react with the oxygen carrier and reduce it. The reduced particles go through the carbon stripper (CS) before entering the air reactor AR1. This CS has been implemented to separate unburnt carbon compounds from the OC in the case of solid fuels combustion (herein, petcoke combustion).

The solid circulation systems are identical from AR1 to AR2 and from AR2 to FR. The oxygen carrier leaving the reactors (AR1 or AR2) by the bottom enters a pneumatic L-valve of 0.017 m i.d. and 1.1 m height. From that point, the solid is transported through a lift with 0.02 m i.d. and 2.25 m height and then enters a horizontal dilute phase conveying line. Finally, the conveying gas and solid are separated in a cyclone. Then,

the OC particles go through a loop seal upstream the next reactor (AR2 or FR). This loop seal, fluidized with nitrogen, allows to avoid any gas transfer between the reactor gas phase and the conveying gas transporting the solid to the cyclone. Between the FR and AR1 the solid leaving the reactor by the bottom goes through a pneumatic L-valve and is transported to the carbon stripper through a lift. The carbon stripper separates the particles according to their volume and density, the lightest particles get entrained by the gas, while the heaviest fall down, leave the carbon stripper by the bottom and enter a loop seal connected to the air reactor AR1.

The fuel reactor (FR) has an internal diameter of 0.13 m and is fluidized with nitrogen and methane in gas combustion mode, or nitrogen and water vapour in solid combustion mode. The total flow rate of the fluidizing gas is chosen in order to operate at 3 times the minimum fluidization velocity of the OC to ensure a sufficient fluidisation. Both air reactors (AR1 and AR2) can be fed with air or nitrogen. As in the fuel reactor, the total flow rates used are chosen to obtain a good fluidisation of the particles.

The CLC pilot unit is equipped with three multi-gas online analysers. CH_4, CO and CO_2 concentrations are continuously measured at the outlet of the FR by non-dispersive (NDIR) infrared analysers (ABB-URAS 26), while H_2 concentration is analysed by a thermal conductivity detector (ABB-Aldos 27). In AR1, CO, CO_2 and O_2 concentrations are determined by a combined NDIR-paramagnetic analyser (ABB-Uras 26 /Magnos 206). Finally, in AR_2, O_2 is measured by an electrochemical cell analyser (Siemens – Ultramat 23). All data are collected by means of a PLC which is connected to a computer.

3.4.2 Mass balances

The variation of the concentration of gaseous compounds in bubble and dense phases are represented by the same set of equations as in batch model (equations 2, 3, 4 and 5 in part 3.3.2).

Regarding solid concentration evolution, the bed is divided in two parts as presented in Figure 3-12. From the solid injection to the reactor bottom, the oxygen carrier bed is represented as a plug flow with axial dispersion from top to bottom (equation 28).

$$\mathrm{S}.\varepsilon_s.\frac{\partial \mathrm{C}_\mathrm{S}^\mathrm{i}}{\partial \mathrm{t}} = \mathrm{D}_{\mathrm{ax},s}\frac{\partial\left(\varepsilon_\mathrm{S}.\mathrm{S}.\partial \mathrm{C}_\mathrm{S}^\mathrm{i}/\partial \mathrm{z}\right)}{\partial \mathrm{z}} + Q_S\frac{\partial \mathrm{C}_\mathrm{S}^\mathrm{i}}{\partial \mathrm{z}} + \rho_s.\mathrm{S}.\varepsilon_s\sum_\mathrm{j}\mu_{\mathrm{i,j}}.\mathrm{r}_\mathrm{j} \qquad 28$$

With:

Q_S : the solid volumic flow rate (m^3/s),

At the injection point location the following equation 29 is used.

$$\mathrm{S}.\varepsilon_s.\frac{\partial \mathrm{C}_\mathrm{S}^\mathrm{i}}{\partial \mathrm{t}} = \mathrm{D}_{\mathrm{ax},s}\frac{\partial\left(\varepsilon_\mathrm{S}.\mathrm{S}.\partial \mathrm{C}_\mathrm{S}^\mathrm{i}/\partial \mathrm{z}\right)}{\partial \mathrm{z}} + \frac{Q_S\mathrm{C}_{\mathrm{S},inj}^\mathrm{i} - Q_S\mathrm{C}_{\mathrm{S},l}^\mathrm{i}}{dz} + \rho_s.\mathrm{S}.\varepsilon_s\sum_\mathrm{j}\mu_{\mathrm{i,j}}.\mathrm{r}_\mathrm{j} \qquad 29$$

With:

$C_{S,inj}^i$: the injection solid concentration of species *i* (mol/m^3),

Above the solid injection point, only axial dispersion is considered (equation 30).

$$\mathrm{S}.\varepsilon_s.\frac{\partial \mathrm{C}_\mathrm{S}^\mathrm{i}}{\partial \mathrm{t}} = \mathrm{D}_{\mathrm{ax},s}\frac{\partial\left(\varepsilon_\mathrm{S}.\mathrm{S}.\partial \mathrm{C}_\mathrm{S}^\mathrm{i}/\partial \mathrm{z}\right)}{\partial \mathrm{z}} + \rho_s.\mathrm{S}.\varepsilon_s\sum_\mathrm{j}\mu_{\mathrm{i,j}}.\mathrm{r}_\mathrm{j} \qquad 30$$

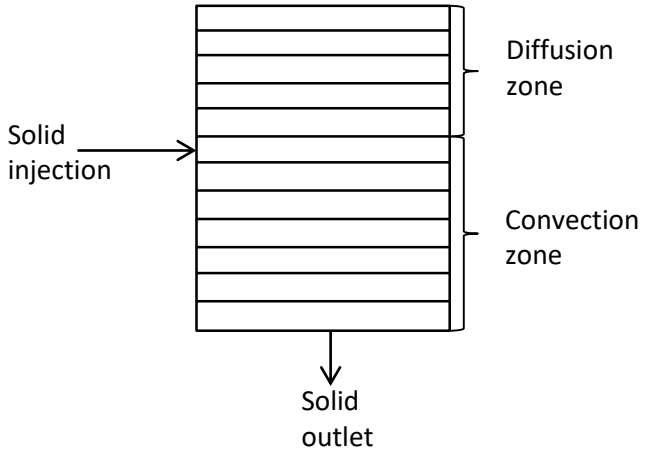

Figure 3-12: Solid circulation in the continuous fluidized bed

These equations are integrated over time to predict the evolution of gas and solid compounds concentration and gas velocity. The hold-ups and the pressure drop are initialized before the integration of these equations and stay unchanged over time to reduce the model stiffness. When more gas goes in the bubble phase, the hold-up will stay unchanged and the bubble gas superficial and real velocities will be impacted. It corresponds to bubbles with a constant size but showing variation of velocity. The kinetic laws used are the ones determined in the batch unit.

3.4.3 Hydrodynamic description

As explained above, the fuel reactor is operated at around 3 times the minimal fluidization velocity of the oxygen carrier. As a consequence, the bubbling bed hydrodynamic correlations presented in part 3.3.3 are still valid.

The mass of oxygen carrier inside the reactor is calculated knowing the bed height and the bed density:

$$m_{OC} = SH_{bed}\rho_{OC} \quad (31)$$

While the petcoke mass in the reactor is estimated using the following correlation 32.

$$m_P = \frac{m_{OC}}{Q'_{OC}} Q'_P \quad (32)$$

With:

Q'_P : the inlet petcoke mass flowrate (kg/s)

Q'_{OC} : the inlet oxygen carrier mass flowrate (kg/s)

In this correlation petcoke mass inside the bed is calculated assuming that the residence time of the petcoke is equal to one of the oxygen carriers.

3.4.4 Model validation

Using the kinetic parameters determined in the batch unit, the 10 kW pilot model predictions are quite good. ITable 3-3 presents the comparison between the FR outlet concentrations of CO, CO_2, CH_4 and H_2 measured experimentally and calculated with the model after water removal (measure taken after the condenser) for a test with methane as fuel at 940 °C with an oxygen carrier flowrate of 20 kg/h, a bed height of 53 cm and a total inlet gas flowrate of 2.1 Nm^3/h containing 200 NL/h of methane.

Table 3-3: Comparison of model predictions and experimental results for methane conversion at 940 °C in the 10kW IFPEN pilot

	Experiment	Simulation
x_{CH4}	3.94	4.82
x_{CO2}	4.76	4.69
x_{CO}	0.04	0.01
x_{H2}	0.23	0.01
r0dX	1.39	1.37

The r0dX prediction is very close to the experimental value. Accounting for the fact that the methane conversion kinetic parameters have been calibrated using only two points in the batch unit, the model predictions regarding gas phase composition are quite good. Since petcoke gasification is the limiting step in this process, no further points have been acquired to improve the quality of methane conversion predictions.

During the campaign with petcoke, 7 experimental points have been collected. The operating conditions tested are listed in Table 3-4.

Table 3-4: Operating conditions of the tests performed with petcoke in the 10 kW continuous unit

Balance	Steam content	Petcoke flowrate	Temperature	OC flowrate	Bed height
-	%	g/h	°C	kg/h	cm
ref	49	117	927	20	53
T	50	110	904	21	55
QP	50	258	928	21	51
Hbed	50	114	929	22	66
T	50	120	894	21	52
xH2O	31	115	929	21	51
QOC	50	119	922	10	51

The parity diagrams of petcoke conversion, r0dX value and carbon dioxide outlet fraction are presented in Figure 3-13. **Without any modification of the petcoke kinetics calibrated in the batch unit, the model predictions for the continuous unit are within 10 % uncertainty for most of the tests, which is a very good result.** This uncertainty is in line with the experimental accuracy.

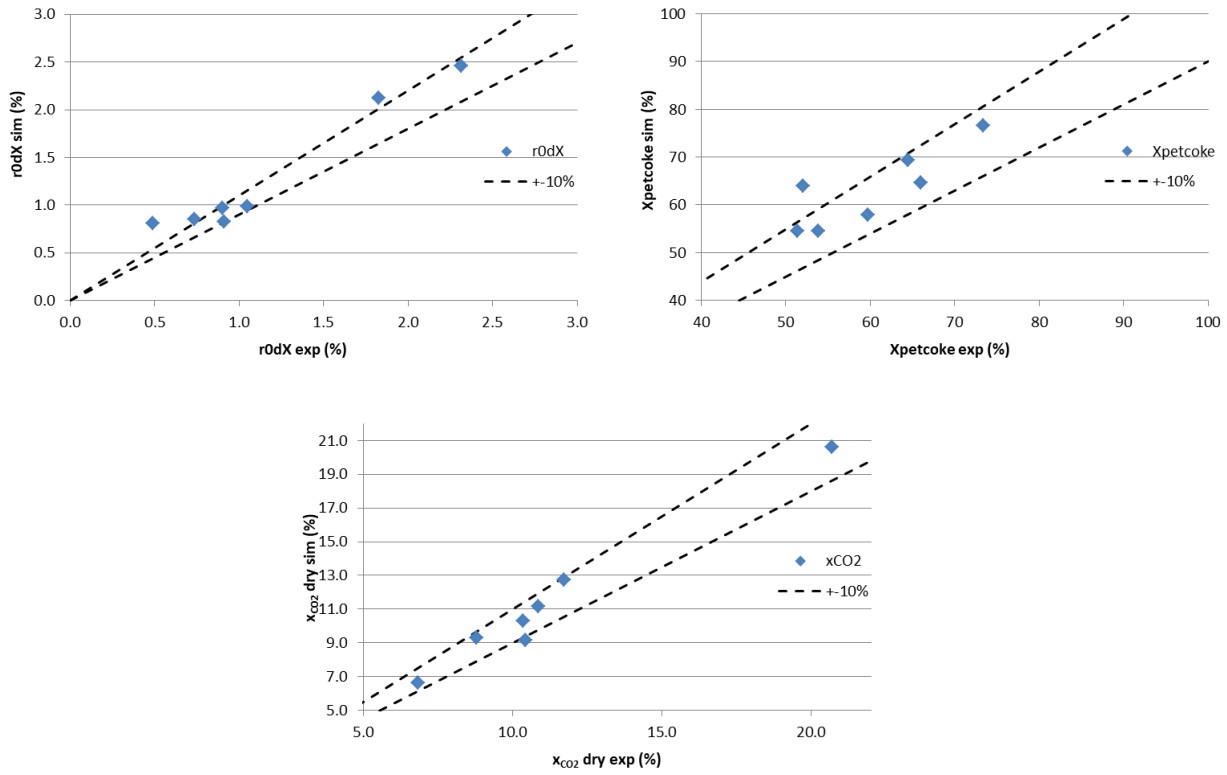

Figure 3-13: Parity diagram of r0dX, $X_{petcoke}$ and x_{CO2} for tests with petcoke in the 10 kW pilot modelling.

The model extrapolation to the CHEERS demonstration unit and an industrial scale unit will now be discussed.

3.5 Turbulent fluidized bed reactor model

3.5.1 CHEERS demonstration unit and industrial scale unit representation

Figure 3-14 presents the design of the CHEERS demonstration unit as proposed in deliverable D2.3 which is representative of an industrial unit. In this design a turbulent fluidized bed reactor is used to ensure a sufficient solid residence time to convert petcoke. The solids and gases are conveyed from the reactor to the carbon stripper through a riser. The role of the carbon stripper is to separate the oxygen carrier from the gas and petcoke. Petcoke is then separated from the gas through a cyclone and recycled to the turbulent bed.

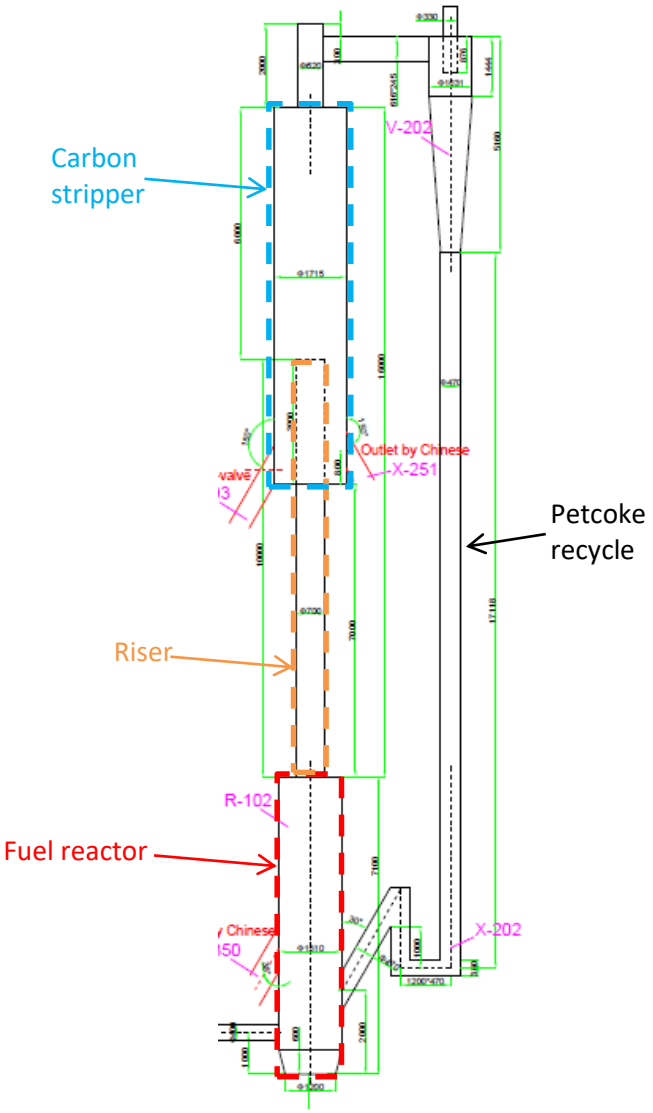

Figure 3-14: CHEERS demonstration unit Fuel reactor design from deliverable D2.3.

In the next part the models proposed for the turbulent bed reactor are presented. These models will be validated using the experimental results acquired in the CHEERS demonstration unit.

3.5.2 Turbulent bed hydrodynamic description

The modelling of a turbulent fluidized bed reactor is quite close to a bubbling bed model. During its PhD at Hamburg university, founded by TOTAL, T. Wytrwat has proven that the 2 phases approach can still be used to represent a turbulent bed reactor [8]. But the correlations used to predict gas velocity, mass transfers and gas and solid hold ups have to be modified to better fit the experimental data. Thus, new correlations must be used for the hold-up calculations, mass transfer coefficient, gas superficial velocity and pressure drop calculations, but the mass balances equations proposed for the bubbling bed reactors stay unchanged.

3.5.2.1 Axial dispersion coefficients

The gas axial dispersion coefficient can be calculated from two correlations. And one correlation was found for the solid axial dispersion coefficient. The domain of validity of these correlations is either partially out of range of our study or not provided. All correlations will be compared and validated when CHEERS demonstration unit experimental results will be available.

a) Correlation of Foka 1996 [9]

$$Pe = \frac{V_{sg,d} H_{bed}}{D_{ax,g}} = 7 * 10^{-2} Ar^{0.32} \left(d_p / D_R\right)^{-0.4} \quad (33)$$

With:

$$\mathrm{Ar} = \frac{\mathrm{g.d_p^3 \rho_g \left(\rho_{OC} - \rho_g\right)}}{\mu_g^{\ 2}} \quad (34)$$

The domain of validity of this correlation is:

$$2 \leq Ar \leq 216$$
$$510 \leq D/d_p \leq 2667$$
$$T \leq 600°C$$

b) Correlation provided by Thompson et al. [10].

$$Pe = \frac{V_{sg,d} H_{bed}}{D_{ax,g}} = 0.247 Ar^{0.32} \left(\frac{D_R}{d_p}\right)^{0.02344} Sc^{-0.2317} \left(\frac{H_{bed}}{D_R}\right)^{0.2854} \quad (35)$$

With:

$$Sc = \frac{\mu_g}{\rho_g D_{m,g}} \quad (36)$$

c) Correlation of Lee and Kim 1990 [11]

$$D_{ax,s} = \frac{\left(V_{sg} - U_{mf,OC}\right) D_R}{\left(1 - \varepsilon_{gd} - \varepsilon_{gb}\right) 4.222 \times 10^{-3}\, Ar} \quad (37)$$

This correlation has been calibrated for Arrhenius number greater than 184 and lower than 33500 and for a superficial gas velocity lower than 1.3 m/s.

3.5.2.2 Mass transfer coefficient between bubble and dense phase

To calculate the mass transfer coefficient between bubble and dense phase, three correlations will be compared:

a) The correlation proposed by Foka et al. [12].

$$K_{bd} = k_{bd} a_b = \frac{Sc^{0.37} V_{sg}}{0.613} \quad (38)$$

This correlation has been defined for the following range of operating conditions:

- $V_{sg} \leq 2.6\ m/s$
- $0.1m \leq D \leq 0.2m$
- $75\mu m \leq d_p \leq 200\mu m$
- $\frac{570kg}{m^3} \leq \rho_s \leq \frac{2650kg}{m^3}$
- $H_0 = 0.5m$

The range of diameter does not cover the CHEERS and industrial scale dimensions. Nevertheless, this correlation will be extrapolated and validated with the CHEERS demonstration unit results.

b) The correlation proposed by Vepsäläinen [13].

$$k_{bd} = 1.74 * 10^{-4} Sc^{0.81} \frac{D_{m,g}}{d_p} \quad (39)$$

The bubble/void specific surface a_b is given by equation 40 assuming long cylindrical bubbles/voids.

$$a_b = \frac{4}{d_b} \quad (40)$$

The bubble/void diameter d_b is estimated using equation 41 determined by T. Wytrwat work [7].

$$d_b = 0.6 l_p \frac{4}{3} g \frac{l_p}{u_{gb}^2} \quad (41)$$

With:

l_p: the bubble piercing length (m)

u_{gb}: the bubble/void velocity (m/s)

These parameters are both provided by correlations which are not provided in this deliverable for confidentiality reasons.

c) The correlation proposed by Thompson et al. [14].

$$k_{bd} = 2.023 \left(\frac{U_{mf}}{3} + 2 \sqrt{\frac{D_m \varepsilon_{mf} U_b}{\pi d_b}} \right) \quad (42)$$

The prediction of the mass transfer coefficient for these three correlations will be compared and the most appropriate one will be selected after validation with the CHEERS demonstration unit experimental results.

3.5.2.3 Gas superficial velocity calculation

From the experiments, carried out in a turbulent bed reactor during the PhD of Tom Wytrwat at Hamburg university, the real gas velocity in dense phase has been calculated from the Ergun equation as shown in equation 43. The dense and bubble phases gas superficial velocity are calculated from the real gas velocity in dense phase through equations 44 and 45.

$$U = -\frac{75}{1.75}\left(1-\frac{\varepsilon_{gd}}{\varepsilon_{gd}+\varepsilon_S}\right)\frac{\mu_g}{\rho_g d_p} + \sqrt{\left(\frac{75}{1.75}\left(1-\frac{\varepsilon_{gd}}{\varepsilon_{gd}+\varepsilon_S}\right)\frac{\mu_g}{\rho_g d_p}\right)^2 + \frac{150}{1.75}\frac{(1-\varepsilon_{mf})\left(\frac{\varepsilon_{gd}}{\varepsilon_{gd}+\varepsilon_S}\right)^3}{{\varepsilon_{mf}}^3}\frac{\mu_g}{\rho_g d_p}U_{mf,OC} + \frac{\left(\frac{\varepsilon_{gd}}{\varepsilon_{gd}+\varepsilon_S}\right)^3}{{\varepsilon_{mf}}^3}{U_{mf,OC}}^2} \quad (43)$$

$$V_{sg,d} = U\varepsilon_{gd} \quad (44)$$

$$V_{sg,b} = V_{sg} - V_{sg,d} \quad (45)$$

3.5.2.4 Hold-ups calculation

The holdup calculations are now calculated with the following methodology:

- Calculation of the axial dispersion coefficients (correlations part 0)
- Calculation of the mass transfer coefficient between bubble and dense phase (correlations part 0)
- Calculation of the gas total superficial velocity (equation 5 part 3.3.2)
- Calculation of gas superficial velocity in dense and bubble phases (equations part 3.5.2.3)
- Calculation of the minimal fluidization velocity (correlations part 3.3.3.3)
- Calculation of the dense gas and solid hold-ups with correlations from T. Wytrwat which are not provided in this deliverable for confidentiality reason .

These hold-ups are initialized at the beginning of a simulation and are not changed later. The ratio of petcoke and oxygen carrier mass is calculated using initial values before reaction. An initial homogeneous petcoke distribution is supposed in the model.

3.5.2.5 Bed pressure drop

The bed pressure drop observed for a difference of height dz is calculated from the following set of equations:

$$\Delta P = \Delta P_{hyd,g} + \Delta P_{hyd,s} + \Delta P_{fric,g} + \Delta P_{fric,s} \quad (46)$$

With:

- the hydrostatic pressure drops:

$$\Delta P_{hyd,g} = \rho_g\left(\varepsilon_{gb}+\varepsilon_{gd}\right)g dz \quad (47)$$

$$\Delta P_{hyd,s} = \rho_s \varepsilon_S g dz \quad (48)$$

- the pressure drop due to gas friction taken from the VDI-heat atlas 2010 [15]:

$$\Delta P_{fric,g} = f_g \frac{dz}{D_R} \frac{\rho_g}{2} \left(\varepsilon_{gb} + \varepsilon_{gd}\right) {V_{sg}}^2 \quad (49)$$

With three potential correlations for f_g:

a) Monazam et al. 2010 [16]:

$$f_g = 0.0056 + 0.5(Re)^{0.32} \quad (50)$$

b) Blasius [17]:

$$f_g = 0.3164\, Re^{-0.25} \quad (51)$$

c) VDI-heat atlas [15]:

$$f_g = 0.006 + \frac{0.55}{Re^{1/3}} \quad (52)$$

- the pressure drop due to solid friction according to Monazam et al. 2010 [15]:

$$\Delta P_{fric,s} = f_s \frac{dz}{D_R} \frac{\dot{Q}_s}{2} \quad (53)$$

With:

$\dot{Q}_s$: the solid mass flow rate over reactor section (kg/m²/s)

f_s is given by the following correlation:

$$f_s = 0.0285(gD_R)^{0.5} \quad (54)$$

3.5.3 Model validation

The equations proposed in the previous parts have been implemented in the code. The dense turbulent bed model is now ready to be validated with future CHEERS pilot experimental results.

The design of the CHEERS demonstration unit has been done targeting 60 % of petcoke conversion in one through. The necessary petcoke residence time has been estimated using batch pilot measurements. By simulating the CHEERS demonstration unit, using the design proposed in deliverable D2.3, a petcoke conversion of 64.7 % is estimated. **The hypotheses taken by the design team are thus is line with the model prediction**.

3.6 Conclusion

In this report, the mechanism of petcoke gasification has been defined with the use of experiments performed in fixed bed reactor with ilmenite as oxygen carrier. It has been proven experimentally that petcoke is progressively consumed from the inside by water during gasification, which leads to a progressive increase of the petcoke porosity and a decrease of its density over time. The particle radius is assumed to be constant in the model even though a small decrease has been observed experimentally. Carbon dioxide does not seem to impact petcoke gasification rate.

The comparison between fixed bed and fluidized bed reactor experiments has indicated that petcoke gasification rate is impacted by the oxygen carrier. This impact is linked to the fact that the oxygen carrier oxidizes the produced hydrogen to ensure a constant steam content along reactor height and to a solid/solid interaction between petcoke and oxygen carrier. It was not possible to record independently the solid/solid interaction reaction but to have a more representative reaction rate it was decided to perform the kinetic measurements in the batch fluidized bed reactor. An apparent gasification kinetic is thus considered here.

Using the kinetic laws calibrated with the batch bubbling fluidized bed reactor, the IFPEN 10 kW pilot plant operated in continuous reactor was modelled and a very good quality of prediction was obtained. These results validate the kinetic laws proposed.

Finally, using the results of Tom Wytrwat doing its PhD, founded by TOTAL, at Hamburg university, a turbulent hydrodynamic is included in the model to propose a simulation tool representative of the CHEERS demonstration unit and industrial scale unit.

4 PART C: CHARACTERISTICS AND PERFORMANCE MODELLING OF OXYGEN CARRIERS

4.1 Introduction

The novelty of the Chemical Looping Combustion (CLC) process is the use of a Metal (Me)/Metal oxide (MeO) system to separate oxygen from air and combust fuel in a nitrogen free environment in a set of two interconnected reactors. The overall performance of the process, both thermodynamic and techno-economic, is dependent on the oxygen carrier (OC) system utilized in the process and a subsequent design of the process conditions. The choice of the OC thus plays a critical role.

The approach to select a suitable OC is typically based on engineering judgement and expertise based on earlier work or a survey of open literature. Important performance factors are high reactivity in the fuel and air reactors, minimizing residence time and reactor size, stability regarding chemical performance over time, efficient separation from ash and char, high attrition resistance, low toxicity, low price, and ease of production (availability). Experiments are performed on a set of selected OCs before choosing the appropriate one for the process under consideration. This is also the chosen approach in the CHEERS project. However, this can be done only for a few selected OCs. How do we arrive at the selected OCs? Or in other words, can we screen all possible or, more practically, a large number of OCs to arrive at a short list of suitable candidates?

This work proposes to develop a thermodynamic screening methodology to identify or rank a set of OCs based on their performance and to provide insights into the suitable operating condition of each OCs. This work is a first step in a more exhaustive approach for screen OCs from a thermodynamic and techno-economic perspective.

4.1.1 Process description and oxygen carrier systems

4.1.1.1 Process description

Figure 4-1 shows the flow diagram for the analysed chemical looping combustion (CLC) process. This work focuses on the effect of the oxygen carrier (OC) and not on the design of the process. Therefore, the actual process set-up does not affect the results of this study, but a conceptual framework is necessary to analyse the effect of the OC in the potential for power production. In CLC, reduced OC (Me) enters the air reactor (AR), where it is oxidized in an exothermic reaction. The AR can be operated isothermally, and in that case the recovered heat can be used directly to produce steam[1]. Oxidized oxygen carrier (MeO) enters the fuel reactor, providing the oxygen for combustion. Steam or recycled flue gas, containing mostly steam and CO_2, are necessary to maintain the appropriate fluidization regime in the FR. When solid fuels such as petcoke are used, steam, and to a lesser extent CO_2, also serve as a gasifying agents, such that the gasification products react with the OC. The fuel reactor typically operates adiabatically, heat is extracted from the flue gases.

The solid fuel also contains an inorganic fraction and will generate ashes. Moreover, as gasification is limited by kinetics [18], it may not be complete, and char has to be separated from the OC when leaving the FR. Thus, the pilot set-up includes a carbon stripper [19], from which heat can also be removed, which is not considered in this conceptual layout. In addition, an oxygen polishing step for the flue gas is required

[1] As mentioned later, in the CHEERS design, heat is mainly recovered from the depleted air, FR flue gases and carbon stripper.

to burn the incomplete combustion products (CO and H_2). The concentration of incomplete combustion products in the flue gas will depend on several factors such as reactor design (residence time, contact) and the nature of the OC. In this work, we explore the effect of the thermodynamic equilibrium with different oxygen carriers.

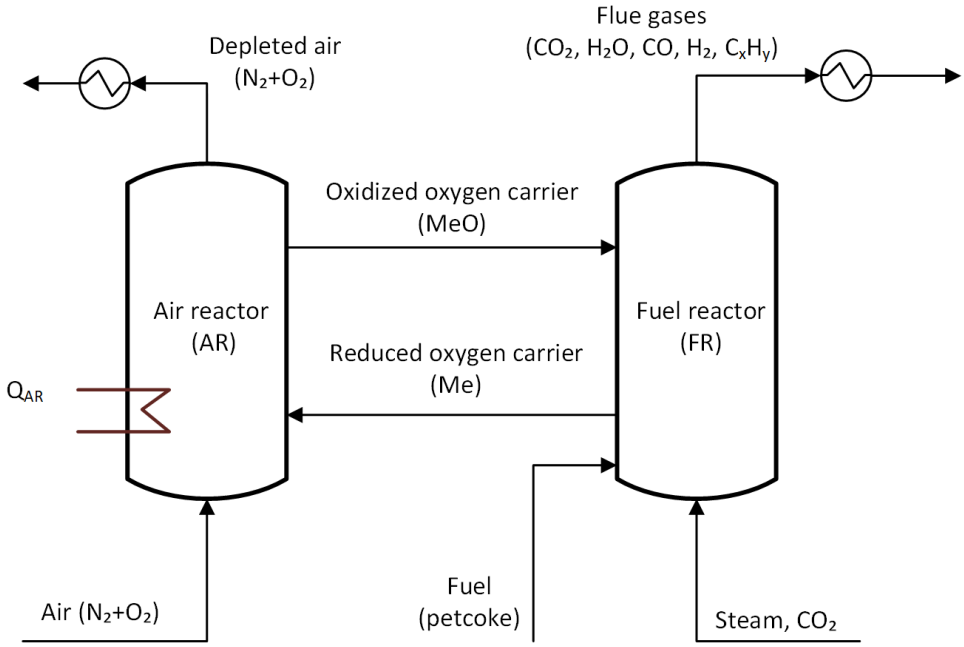

Figure 4-1 Chemical looping combustion process flow diagram considered in this analysis

4.1.1.2 Gasification

The overall reaction occurring in the FR is

$$\underbrace{\text{solid fuel}}_{\text{C,H, O, (N, S)}} + OC + CO_2(g) + H_2O\ (g) \rightarrow CO\ (g) + H_2(g) + CO_2(g) + H_2O\ (g)$$

The two occurring gasification reactions are:

$$C + CO_2 \rightarrow 2CO \qquad \Delta H = 170 kJ/mol\ C$$

$$C + H_2O \rightarrow CO + H_2 \qquad \Delta H = 135 kJ/mol\ C$$

From previous experiments within CHEERS, it has been observed that steam gasification is dominant. In this analysis, we calculate the gasification products using equilibrium thermodynamics.

4.1.1.3 Analysed oxygen carriers- redox reactions

The four oxygen carrier systems considered in this study are:

Copper/Copper oxide

$$CuO \rightarrow Cu + \frac{1}{2}O_2$$

Nickel/Nickel oxide

$$NiO \rightarrow Ni + \frac{1}{2}O_2$$

Iron (III) oxide/Iron (II, III) oxide

$$3Fe_2O_3 \rightarrow 2Fe_3O_4 + \frac{1}{2}O_2$$

Pseudobrookite, Rutile/Ilmenite

$$Fe_2TiO_5 + TiO_2 \rightarrow 2FeTiO_3 + \frac{1}{2}O_2$$

As ilmenite is a natural ore, several species may be present. The FR operates at 950 °C and only species existing at higher temperatures, pseudobrookite (Fe_2TiO_5), rutile (TiO_2) and ilmenite ($FeTiO_3$), are considered within this study. The reaction considered within this study is reported in [20], [21].

4.2 Methodology

Figure 4-2 shows the workflow used in this analysis to estimate the potential for power production using different oxygen carriers based on equilibrium calculations. As explained later, in Section 4.2.2, the fuel reactor is modelled as two sections, where the first one corresponds to the gasification reactions and the second one to the combustion with the oxygen carrier. The petcoke flowrate and composition, together with the steam and CO_2 flowrate are used to calculate the equilibrium composition of the gasified fuel, which is used in the mass and energy balance. The fuel reactor equilibrium conversion, which is also used in the CLC mass and energy balance, is calculated considering the flowrates of petcoke, steam, CO_2 and oxygen carrier to the fuel reactor. An estimate of the available heat for recovery is obtained from the CLC mass and energy balance, and then used to estimate the power production based on exergy efficiency.

The model used for the equilibrium calculations is explained in Section 4.2.1, while the estimation of available heat and power production is explained in Section 4.2.2.

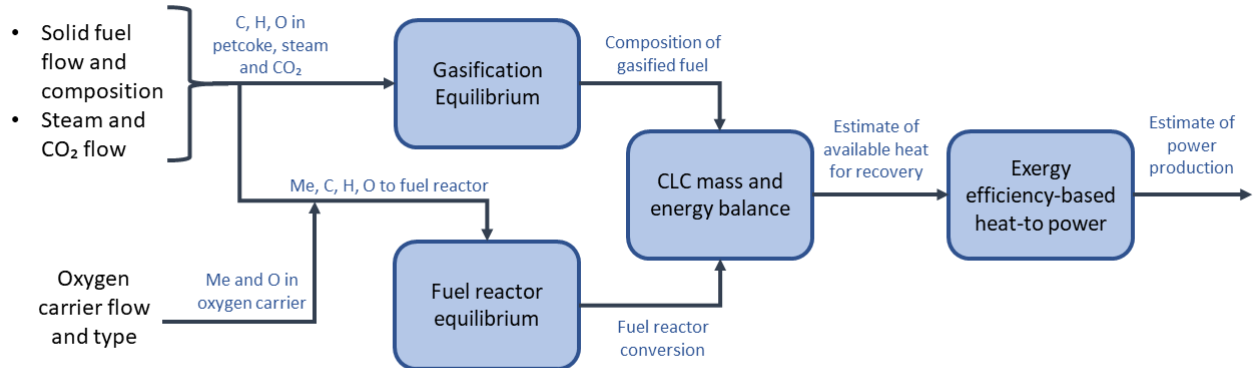

Figure 4-2 Workflow for estimating the potential for power production using different oxygen carriers

4.2.1 Equilibrium calculations

Equilibrium concentrations can be calculated by minimizing the Gibbs free energy of all the species that may be present in the system. This approach has been used successfully for processes involving a large number of possible reactions [22]–[24].

4.2.1.1 Gibbs Free Energy minimization

4.2.1.1.1. Definition of the minimization problem

The equilibrium composition can be calculated by solving the minimization problem in Equation 1, where the objective function is the Gibbs free energy (G), subject to the element balance.

$$min \quad G = \Sigma n_{i \forall gas}\left[G^{o}_{i \forall gas} + RT\ log\left(y_{i \forall gas}\right)\right] + \Sigma n_{i \forall solid}\left[G^{o}_{i \forall solid} + RT\ log\left(x_{i \forall solid}\right)\right]$$

Equation 1

$$s.t. \sum_{i=1}^{N} a_{ij} n_i = A_j$$

where

i= species: C, H_2O, CO_2, H_2, CO, CH_4, Me, MeO

j= elements: carbon, hydrogen, oxygen, metal

a_{ij} = number of elements j in species i

A_j = number of elements j in the feed

n_i = moles of species i at equilibrium

y_i = concentration of species i in the gas phase at equilibrium

x_i = concentration of species i in the solid phase at equilibrium ($n_i/\Sigma n_i$)

The Gibbs free energy for species *i* can be calculated with Equation 2, using the enthalpy (H) and entropy (S), both of which are a function of temperature (T):

$$G_i^o = H_i^o(T) - TS_i^o(T)$$ Equation 2

This optimization approach has been used in gasifiers [25], [26] and can be applied to both the air and fuel reactors. The parameters that can be varied are temperature (T), and the elements in the feed (A_j). Figure 4-3 depicts the inputs and outputs to the minimization problem when calculating the equilibrium in the FR.

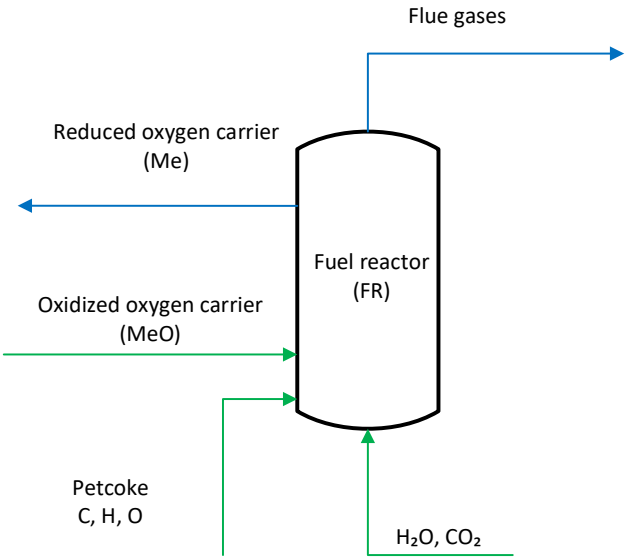

Figure 4-3 Inputs (green) and outputs (blue) for FR equilibrium calculations

There is the possibility that some species are not present at equilibrium. This would cause *log(x)* in Equation 1 to be undefined and cause numerical issues. This can be overcome by adding non-negativity constraints to n_i. An alternative is to perform the variable transformation in Equation 3 [24]:

$$n_i = e^{n_i'}$$ Equation 3

where n_i' is the variable used for optimization.

With this variable transformation, the minimization problem is then

$$\frac{G}{RT} = \sum_{i=1}^{N} e^{n_i'} \left[\frac{G_i^o}{RT} + n_i' - ln\left(\sum_{i=1}^{N} e^{n_i'} \right) \right] \qquad \text{Equation 4}$$

$$s.t. \sum_{i=1}^{N} a_{ij} e^{n_i'} = A_j$$

It has been observed that for this type of systems, this implementation behaves as a convex problem [23], [24], [27][2]. The minimization results presented in this report were obtained using interior-point algorithms[3] [28]–[30].

4.2.1.2 Validation of calculations

4.2.1.2.1. Validation against FactSage

Gibbs free energy minimization is a useful approach to predict the equilibrium composition of a reactor. However, depending on the optimization method and options[4] applied to minimize Gibbs free energy, there may be variations in the numerical solutions, introducing errors on the equilibrium composition. Thus, the results from the constrained minimization of the Gibbs free energy were compared to the equilibrium results from a commercial tool, FactSage [31], to verify the optimization methods used in this work. FactSage [31] is an integrated database for chemical thermodynamics that allows the user to specify a system and calculates the equilibrium composition. For the verification, the following cases were specified (operating temperature of the reactor at 950 °C for Case 1 to 8):

1. OC to provide oxygen to form CO_2 and H_2O from C in petcoke and gasification stream: 2 moles of H_2O and 2 moles of CO_2/mol of C
2. 20 % "excess" OC
3. Poor OC environment (50 % of Case 1)
4. Low gasification stream (CO_2 and H_2O), 75 % of Case1
5. High gasification stream (CO_2 and H_2O), 125 % of Case 1
6. "Excess" steam (3.5 times Case 1)
7. Low CO_2/ H_2O (1.5/2.5) in gasification steam
8. High CO_2/ H_2O (2.5/1.5) in gasification steam
9. Low temperature (900 °C)
10. High temperature (1000 °C)

[2]As a means of verification, both global (basin-hopper [35]) and local [28], [30], [35] constrained optimization algorithms were tested. However, the results were the same in all cases for global and local algorithms.

[3] The results with local optimization algorithms Matlab *fmincon* [30] and *ipopt* [28] using algorithm differentiation, implemented with CasADi [29] are consistent.

[4] Options such as step size and tolerances.

In these cases, the amount of steam and CO_2 are varied proportional to the molar flow rate of carbon in the fuel. The main performance parameter used for comparison was the sum of the square of errors, presented in Table 4-1: Equilibrium calculation results with different operating conditions and their deviations compared to FactSage.. The difference in CO_2 concentration at equilibrium and the difference in reduced OC concentration at equilibrium was also reviewed, with similar results. It can be noted that the difference in results between the realized equilibrium calculation and FactSage is small. The largest difference is observed for the ilmenite system and this is attributed to the fact that the equilibrium calculations only consider the most relevant components (pseudobrookite, rutile and ilmenite), while FactSage considers a larger number of possible compounds and calculates small concentrations of other components, such as Fe_3O_4.

Table 4-1: Equilibrium calculation results with different operating conditions and their deviations compared to FactSage.

Case	Temperature	Molar flow ratio				Difference**			
		C in fuel	OC*	steam	CO_2	Cu/CuO	Ni/NiO	Fe_2O_3/Fe_3O_4	Ilmenite
Case 1	950 °C	1	2.04	2	2	0,01 %	0,01 %	0,10 %	3,52 %
Case 2	950 °C	1	2.44	2	2	0,06 %	0,28 %	0,09 %	3,67 %
Case 3	950 °C	1	1.02	2	2	0,01 %	0,01 %	0,01 %	0,98 %
Case 4	950 °C	1	2.04	2	2	0,01 %	0,01 %	0,11 %	3,29 %
Case 5	950 °C	1	2.04	3	3	0,01 %	0,02 %	0,11 %	3,55 %
Case 6	950 °C	1	2.04	7	7	0,00 %	0,52 %	0,11 %	7,89 %
Case 7	950 °C	1	2.04	3	2	0,01 %	0,01 %	0,10 %	3,41 %
Case 8	950 °C	1	2.04	2	3	0,01 %	0,01 %	0,11 %	3,66 %
Case 9	900 °C	1	2.04	2	2	0,01 %	0,01 %	0,11 %	3,03 %
Case 10	1000 °C	1	2.04	2	2	0,01 %	0,02 %	0,10 %	4,05 %

* for Fe3O4, the molar flow ratio values of OC are multiplied by 3.1

** sum of the squares of differences in each component.

4.2.1.2.2. Validation against literature

The results from the equilibrium calculations were also validated against literature, especially for CuO [23]. For the validation, the fuel composition and other operating conditions are set to be close to the literature. Figure 4-4 indicates that the equilibrium composition of the flue gas and solid from this work is similar to the literature in the entire range of the CuO flow rate. The scale of the y-axis is not the same for the reference and this work, as inlet information is missing in the reference. Only a marginal difference in H_2 and CH_4 fraction in the flue gas at low OC/C ratio can be observed, as in the reference only incomplete combustion products are present below ~0.5 moles of CuO, while in our simulations a mixture of complete and incomplete combustion products are produced also with low OC flowrates.

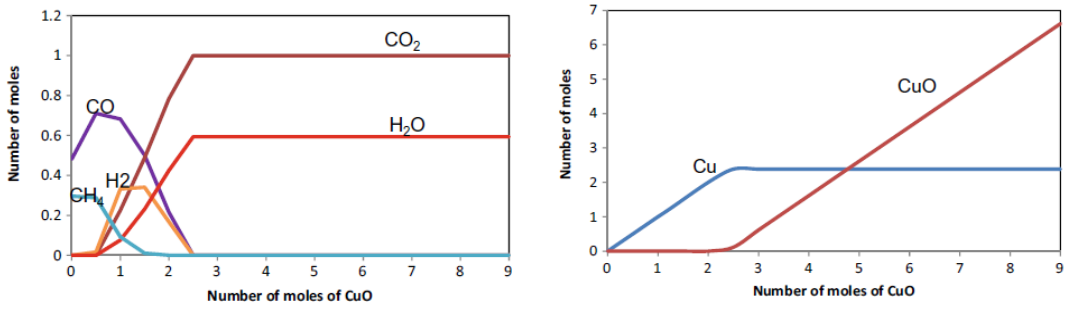

(a) flue gas (right) and solid (left) from literature [23].

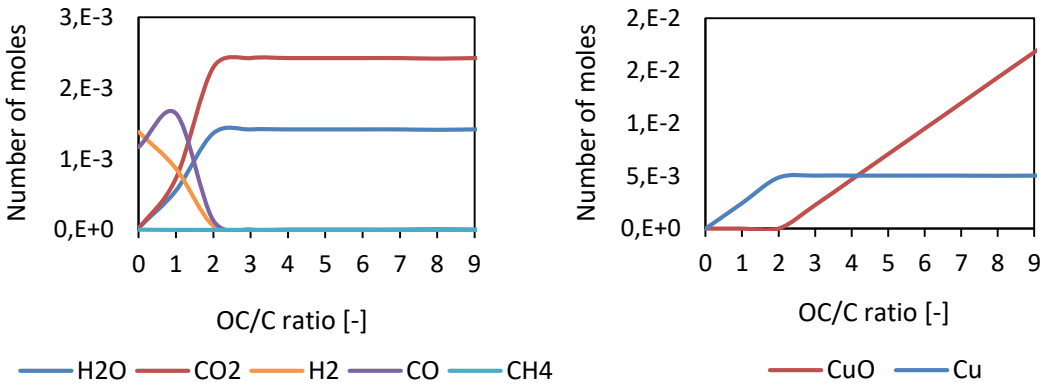

(b) flue gas (right) and solid (left) from this work.

Figure 4-4 Equilibrium calculation results for CLC of coal using CuO with varying OC/C ratio from literature [23] (a) and from this work (b).

4.2.1.3 Parametric analysis

As part of this work, a parametric analysis of the different inputs to the model is performed to investigate the effects of the operating variables on the equilibrium composition of the fuel reactor.

For the sensitivity analysis and comparison of the results, a set of operating conditions, with stochiometric OC for complete combustion, is selected as a base case. The base case operating conditions are described below:

- OC to provide oxygen to form CO_2 from C and H_2O from H in petcoke
- gasification stream: 2 moles of H_2O and 2 moles of CO_2/mol of C.
- Temperature of the fuel reactor: 950°C

The base case is Case 1 in Section 4.2.1.2.1. The analysed parameters are varied with respect to the flowrate of carbon in the petcoke:

- Oxygen carrier flow rate to the FR: varied by oxygen carrier to carbon in petcoke molar ratio (mol of OC/mol of C).
- Steam flow rate to the FR: varied by steam to carbon in petcoke molar ratio (mol H_2O/mol C).
- CO_2 flow rate to the FR: varied by CO_2 to carbon in petcoke ratio (mol CO_2/mol C).
- Temperature of the fuel reactor.

The results of this parametric study are shown in Section 4.3.1.

4.2.2 Estimation of recovered heat and produced power using equilibrium calculations

This section describes the approach to calculate the potential for heat and power, the calculation basis and assumptions for the estimation of available heat and produced power, which is presented in Section 4.3.2.

4.2.2.1 Mass and energy balance – available heat and power

The mass and energy balance is performed for the CLC depicted in Figure 4-1. The fuel reactor is modelled as two sections, as shown in Figure 4-5. Petcoke, steam and CO_2 are fed to the first section, and an equilibrium calculation for the gasification provides the composition of the resulting syngas stream containing H_2, CO, CH_4, H_2O, CO_2, which fed to the second section, in which the combustion with the oxygen carrier occurs. A mass and energy balance is performed in the second lump to estimate the available heat for recovery.

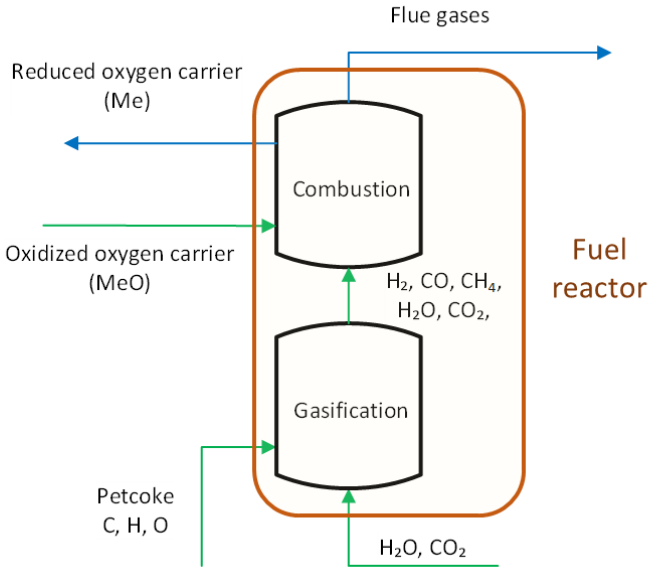

Figure 4-5 Lumped model for fuel reactor.

Conversion factors are calculated from equilibrium calculations for each of the considered oxygen carriers using the methodology described in Section 4.2.1. The calculated conversions are input parameters in the mass and energy balance model, which is used to estimate the heat available for recovery.

To estimate the potential for power production, a heat-to-power conversion with an exergy efficiency of 50 % is assumed, i.e. it is possible to utilize 50 % of the exergy in the recovered heat when converting it to electric power in a steam cycle. In [32], data from a steam cycle producing power from furnace off-gas at approximately 750 °C at a silicon plant in Norway is available. Based on this data, the exergy efficiency of the heat to power conversion is calculated to be 50.4 %, which is close to the value assumed in this work. In [33], an exergy efficiency of 50.7 % was calculated for an ultra-supercritical double reheat steam cycle system.

4.2.2.2 Calculation basis

The equilibrium framework developed in this work was used to estimate the potential for power production of a 3 MW_{th} CLC plant. Considering a LHV of 33565 kJ/kg [19], this corresponds to 321.8 kg/h of petcoke.

For this work, it is considered that petcoke is composed by carbon (C), hydrogen (H) and oxygen (O). The petcoke composition was estimated using the values in the CHEERS Pre-FEED study (D2.3)[19]. The values in

Table 4-2 correspond to the weight composition with C, H, and O.

Table 4-2: Petcoke composition used in this work.

Element	%wt
C	97.6 %
H	1.4 %
O	1.1 %

The flows of metal oxide for each of the oxygen carriers are calculated as the stochiometric flow of oxygen carrier to produce CO_2 and H_2O from the C and the H in petcoke.

In addition to the petcoke and oxygen carrier, 77281 mol/h of a 50 % mol steam/CO_2 flow are fed to the fuel reactor. This is estimated from 1859 Nm^3/h at NPT (20 °C and 101.3 kPa) to the fuel reactor and the carbon stripper in the CHEERS pre-FEED study [19]. It should be highlighted that the oxygen carrier considered for the overall mass and energy balance includes the active metal/metal oxide and the inactive support to accurately account for the energy balance.

4.2.2.3 Main assumptions

The main assumptions for the mass and energy balance and estimation of power production potential are given below:

- Only equilibrium is considered.
- Petcoke only contains carbon (C), hydrogen (H) and oxygen (O).
- Stochiometric flow of metal oxide to produce CO_2 and H_2O from the C and the H in petcoke.
- Air reactor is isothermal at 1000 °C with an air feed temperature of 15 °C
- Conversion in the air reactor is 100 % (only metal oxide is fed to the fuel reactor).
- Fuel reactor is adiabatic with a fuel feed temperature of 30 °C
- Heat for steam production is recovered from air reactor cooling as well as hot gas leaving the air and fuel reactor
    - The hot gases leaving the air and fuel reactor are mixed and cooled to 185 °C. This is similar to the combined cooling from exchanger E-311 and E-313 in the pilot unit [19].
    - Heat from air reactor cooling is available at constant temperature (1000 °C)
- No pre-heating of air is required, since the duty is larger than 2 MW_{th} (following recommendations from Pre-FEED study, D2.3 [19])
- As mentioned earlier, an exergy efficiency of 50 % for heat to power conversion is applied. This is considered to be in the middle of the feasible range for such processes.

4.3 Results

4.3.1 Analysis of equilibrium calculations

In this section, equilibrium calculations in the fuel reactor are performed at different operating conditions (OC/C ratio, Steam/C ratio, CO_2/C ratio, temperature) as discussed in section 4.2.1.3 . This sensitivity study is analysed considering the base case described in 4.2.1.3 and is performed to analyse the effect of variations of different parameters in the equilibrium composition in the fuel reactor.

4.3.1.1 Effect of oxygen carrier/C in petcoke molar ratio

Figure 4-6 presents the results of equilibrium calculations with different oxygen carriers at varying OC/C ratios. The OC/C ratio is ranged from -50 % to +50 % of the base case value. Other operating conditions like the Steam/C ratio, CO_2/C ratio, and temperature are fixed to the base case values. Figure 4-6 shows

incomplete combustion at OC/C ratio below the base case value for all oxygen carriers, resulting in a considerable amount of CO and H_2 in the flue gas. The trace components are reduced with increasing OC/C ratio, reaching to complete combustion. When OC/C ratio is the same as the base case value, complete combustion occurs, giving mainly CO_2 and H_2O in the flue gas. The equilibrium composition does not change with increasing OC/C ratio. Thus, OC/C ratio will not affect the equilibrium calculation in the reactor when OC/C ratio is larger than the base case value. For ilmenite, the complete combustion is delayed until the OC/C ratio value of 3 (the base case value is 2), resulting in a larger flow rate per 1 mole of carbon in petcoke than other oxygen carriers for complete combustion.

4.3.1.2 Effect of steam/C in petcoke molar ratio

During equilibrium calculations, steam to C in petcoke molar ratio is varied from 1 to 3, keeping Steam/ CO_2 ratio constant at 50 %. Other operational variables are set to be the same as the base case. As seen in Figure 4-7, all the oxygen carriers result in complete combustion with varying Steam/C ratios at the base case conditions, giving a CO_2 and H_2O mixture of the flue gas. For ilmenite, however, there is a small amount of CO and H_2 left. As indicated in Section 4.3.1.1 , ilmenite with OC/C ratio of 2, which is the base case value, results in slight incomplete combustion and thus CO and H_2 in the equilibrium composition. The sensitivity analysis also shows that H_2O mole fraction is proportionally increased with the Steam/C ratio as a larger amount of H_2O in the reactor feed will result in a larger amount of unused H_2O left in the flue gas. Thus, only considering the equilibrium and not the impact of the steam addition on the energy balance, and thus, temperature, the change of the Steam/C ratio will not have a significant effect on the equilibrium concentration in the fuel reactor.

4.3.1.3 Effect of temperature

In order to see the effect of the reaction temperature on the equilibrium composition, the operating condition is varied from 800 °C to 1100 °C, considering the base case temperature at 950 °C. Other operational variables are fixed to the base case values. Figure 4-8 presents that complete combustion occurs with all the oxygen carriers in the entire temperature range. The sensitivity analysis also indicates that the reactor temperature has a negligible effect on the equilibrium composition regardless of oxygen carriers, indicating that the increased conversion observed in experimental results (e.g. in [34]) is due to kinetic effects. In the case of ilmenite, rather than an increase in conversion, there is an equilibrium shift between CO_2, CO and H_2 as temperature increases. Figure 4-8d shows that there is CO and H_2 present in the flue gas, meaning incomplete combustion when using stochiometric OC, and a marginal increase in the trace components with temperature. Although, the effect of temperature on the equilibrium composition becomes noticeable in the case of incomplete combustion, the effect is still marginal considering the numerical tolerance of the simulation works.

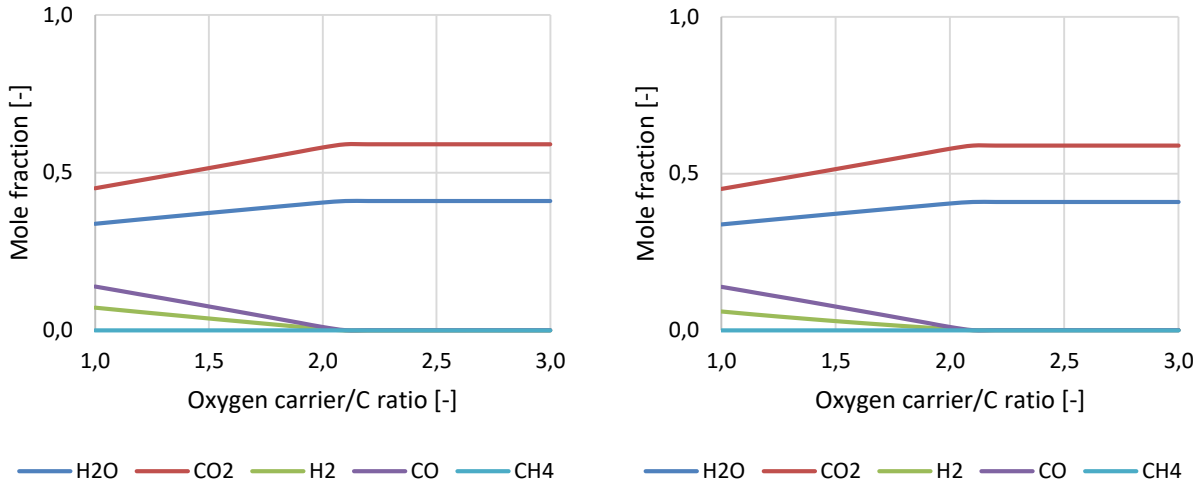

(a) CuO

(b) NiO

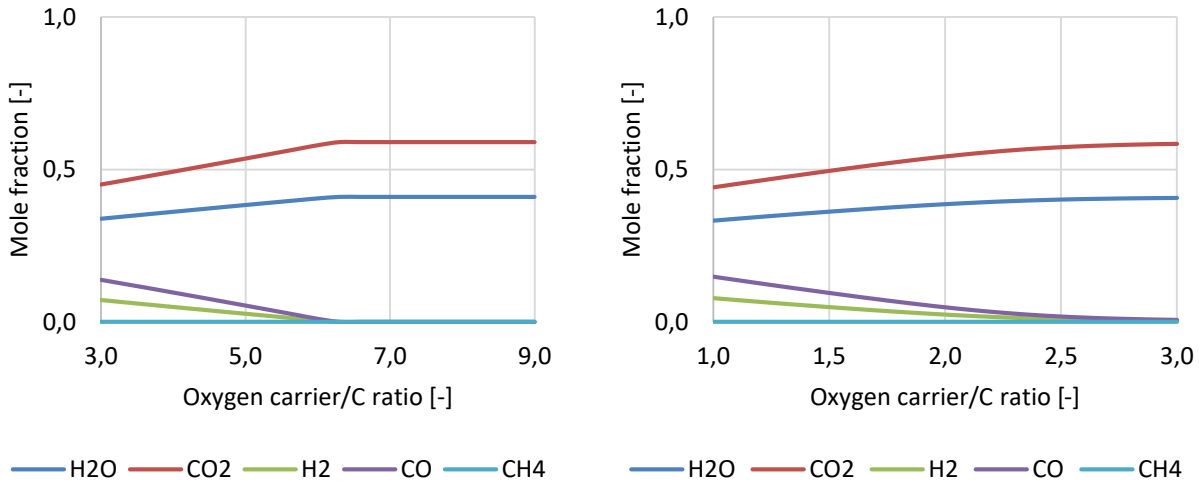

(C) Fe_2O_3

(d) Ilmenite

Figure 4-6 Effect of OC/C ratio on CLC using different oxygen carriers at Steam/C ratio of 2, CO_2/C ratio of 2 and 950 °C.

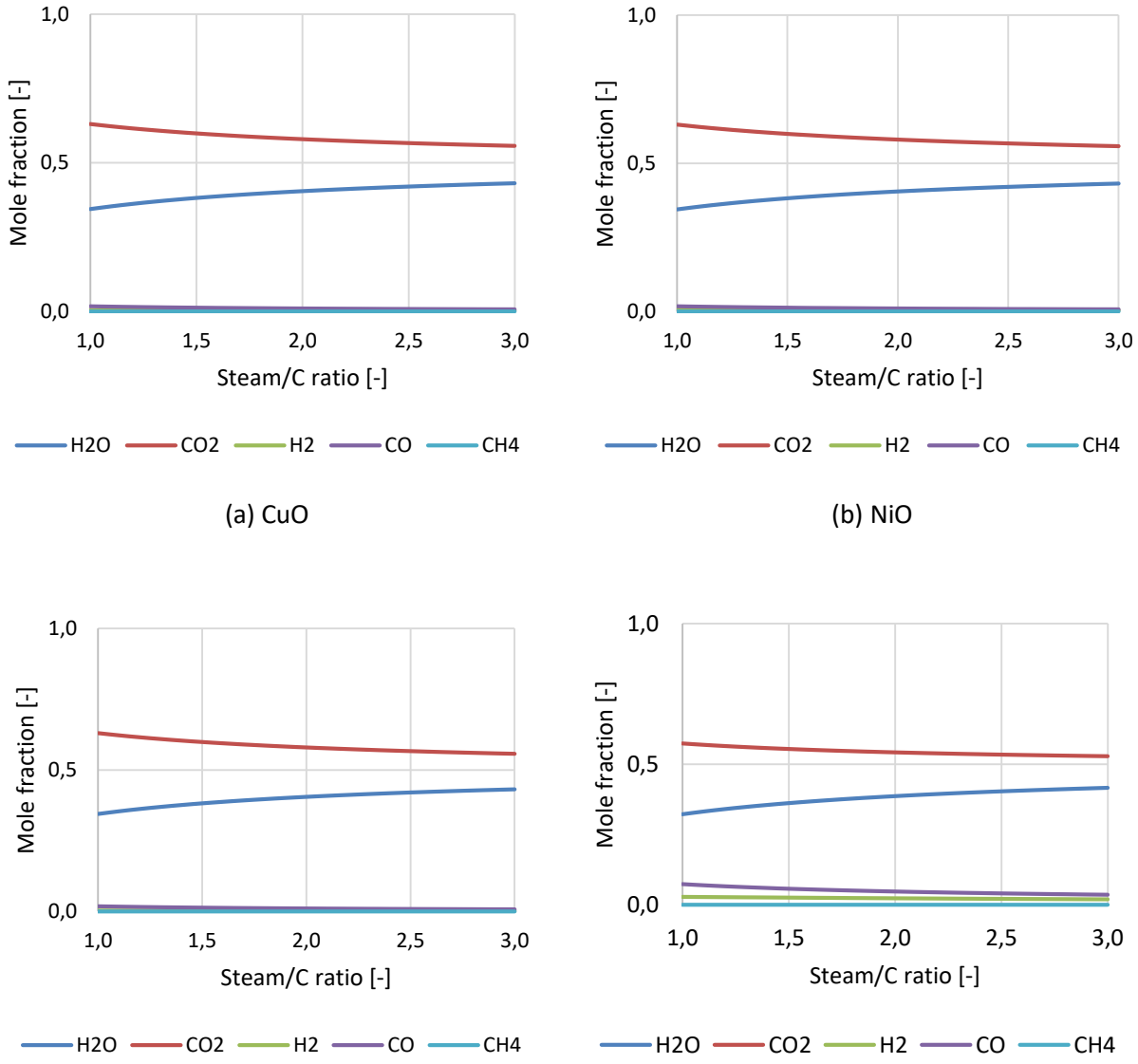

Figure 4-7 Effect of Steam/C ratio on CLC using different oxygen carriers at OC/C ratio of 2 (6 for Fe_2O_3), CO_2/C ratio of 2 and 950 °C.

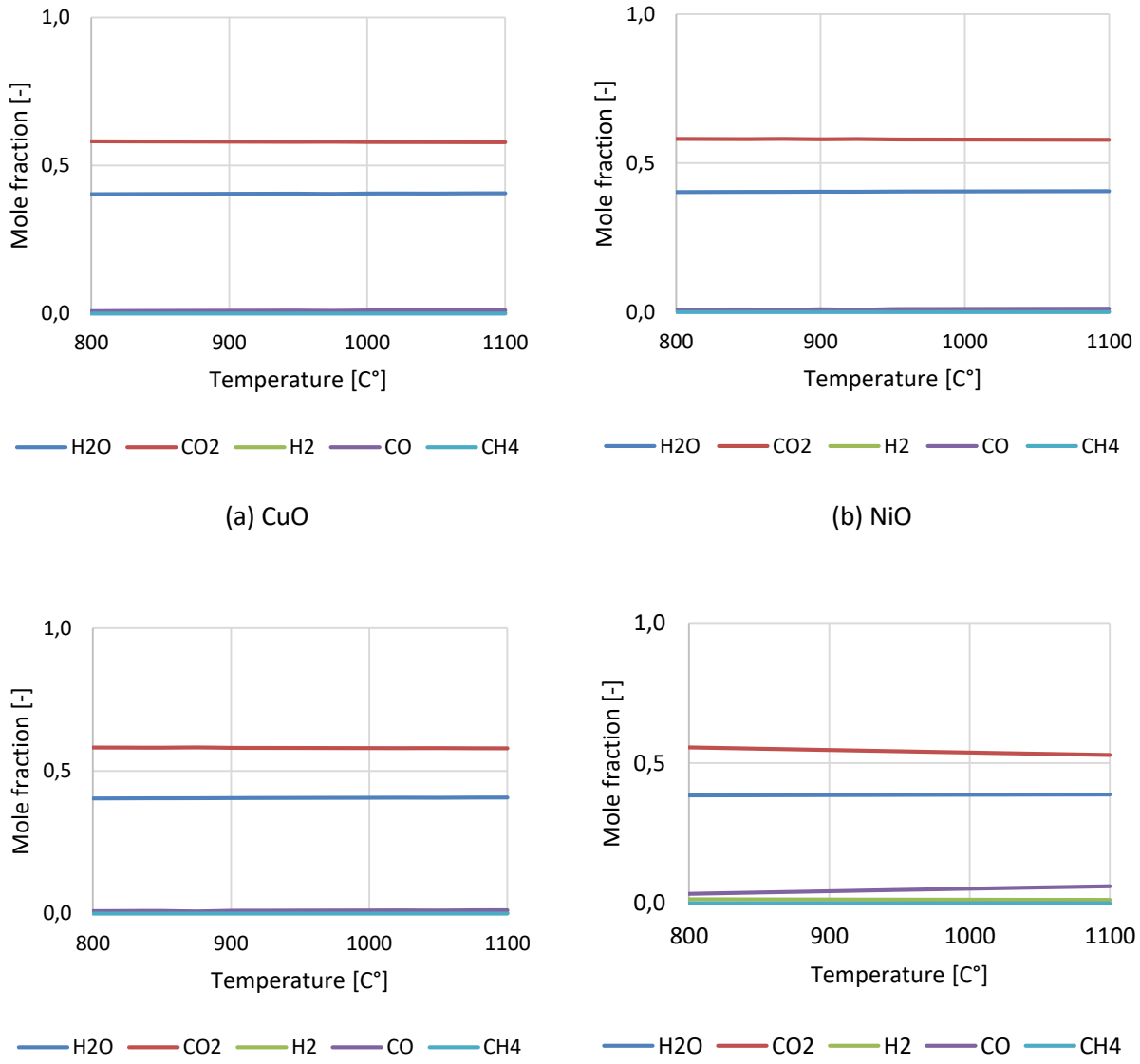

Figure 4-8 Effect of temperature on CLC using different oxygen carriers at OC/C ratio of 2(6 for Fe_2O_3), Steam/C ratio of 2, CO_2/C ratio of 2 and 950 °C.

4.3.1.4 Effect of CO_2/steam ratio

The effect of the CO_2/steam ratio on the equilibrium composition is investigated with different oxygen carriers by varying CO_2/C ratios. CO_2/C ratio is ranged from 1 to 3 (the base case value is 2) in this sensitivity analysis. Other operating conditions of the fuel reactor is set to be the same as the base case. Figure 4-9 shows that CLC with all the oxygen carriers results in the flue gas with mainly CO_2 and H_2O regardless of CO_2/C ratio values. This will mean that at equilibrium, complete combustion will occur at any CO_2/C ratio with the base case conditions. As seen in Figure 4-9, the CO_2 mole fraction is proportionally increased with CO_2/C ratio as a larger amount of CO_2 in the reactor feed will result in a larger amount of unreacted CO_2 left in the flue gas. Therefore, the effect of the CO_2/C ratio on equilibrium calculations will be negligible.

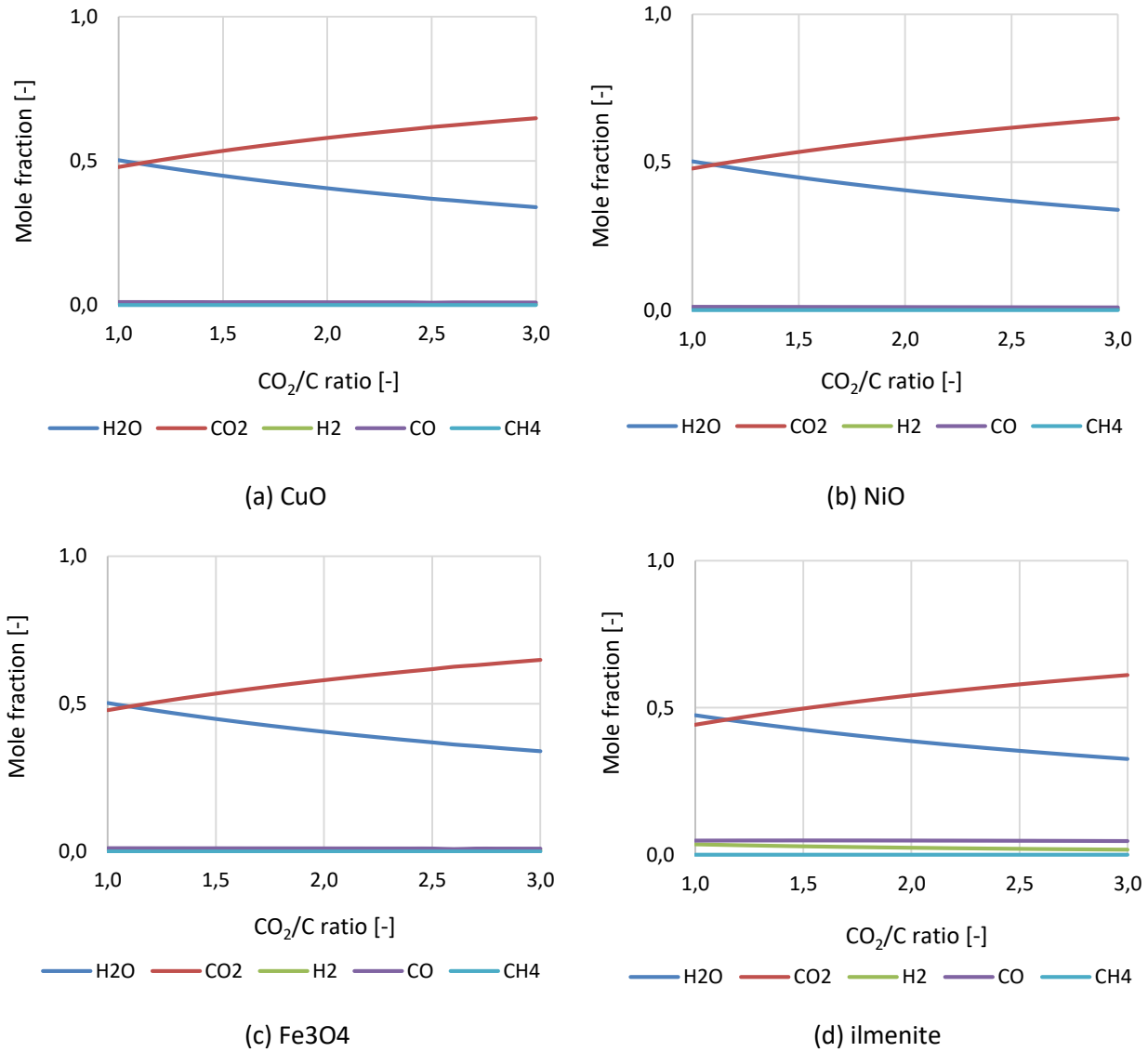

Figure 4-9 Effect of CO_2/C ratio on CLC using different oxygen carriers at OC/C ratio of 2(6 for Fe_2O_3), Steam/C ratio of 2, and 950 °C.

4.3.1.4.1. Effect of OC/C ratio on CLC using CuO with varying CO_2/C ratios

Equilibrium calculations are performed with varying CO_2/C ratio at different OC/C ratios (1, 2, and 3) to investigate the effect of the oxygen carrier flow rate on the changes in equilibrium composition with varying CO_2 flow rates in the feed gas. Other operating conditions of the fuel reactor are set to the base case. Figure 4-10 indicates that the equilibrium composition is almost the same for the OC/C ratio of 3 and 2 in the entire CO_2/C ratio range. However, at the OC/C ratio of 1, H_2O and CO_2 mole fractions are lower than the OC/C ratio of 3 and 2 due to the lack of oxygen and thus resulting in incomplete combustion with CO and H_2 left in the flue gas.

Nevertheless, as seen in Figure 4-10, the differences of the changes in H_2O and CO_2 mole fractions with varying CO_2/C ratios are almost the same for all OC/C ratio values. This trend is also shown in other oxygen carriers (See Figure 6-1, Figure 6-4, Figure 6-7 in section 6 **APPENDIX**). When OC/C ratio is 1, however, CO and H_2 mole fractions are slightly decreased with the CO_2/C ratio. Thus, a higher CO_2/C ratio will be beneficial to have complete combustion when CLC is performed with a low OC/C ratio. Other oxygen carriers also show the same tendency with a low OC/C ratio.

4.3.1.4.2. Effect of CO_2/C ratio on CLC using CuO with varying Steam/C ratios

During equilibrium calculations, the Steam/C ratio is also varied at different CO_2/C ratios (1, 2, and 3). Other operational variables are fixed to the base case values. Figure 4-11 presents that the CO_2 fraction in the entire range of the Steam/C ratio is reduced at a lower CO_2/C ratio, while H_2O fraction shows the opposite trend. As mentioned in section 0, a larger amount of CO_2 in the feed will eventually increase the CO_2 fraction in the equilibrium composition. However, the difference of the changes in the mole fractions of the components with varying Steam/C ratios is nearly identical to all CO_2/C ratio values. In addition, the effect of Steam/C ratio on CLC at different CO_2/C ratios for other oxygen carriers is similar to CuO as seen in Figure 6-2, Figure 6-5, and Figure 6-8 in section 6 **APPENDIX**.

4.3.1.4.3. Effect of CO_2/C ratio on CLC using CuO with varying temperatures

Figure 4-12 presents the results of equilibrium calculations for CLC using CuO with varying temperatures at different CO_2/C ratios (1,2, and 3). Other operational conditions are fixed to be the base case values. As seen in Figure 4-12, the CO_2 fraction is not changed in the entire range of Steam/C ratio, while the fraction is increased at a higher CO_2/C ratio at any temperature. Otherwise, the effect of the CO_2/C ratio on CLC using CuO with varying temperatures is negligible. Other oxygen carriers also present a similar trend to CuO (see Figure 6-3, Figure 6-6, and Figure 6-9 in section 6 **APPENDIX**).

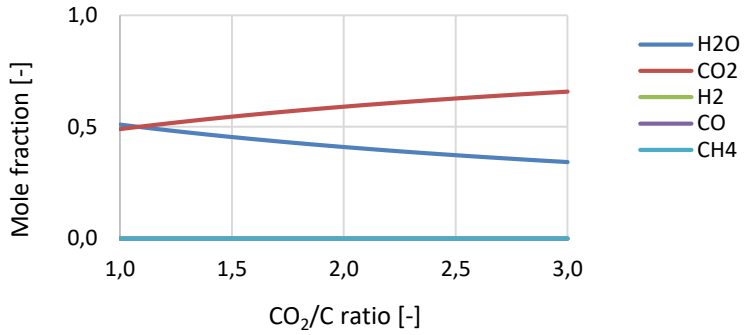

(a) OC/C ratio of 3

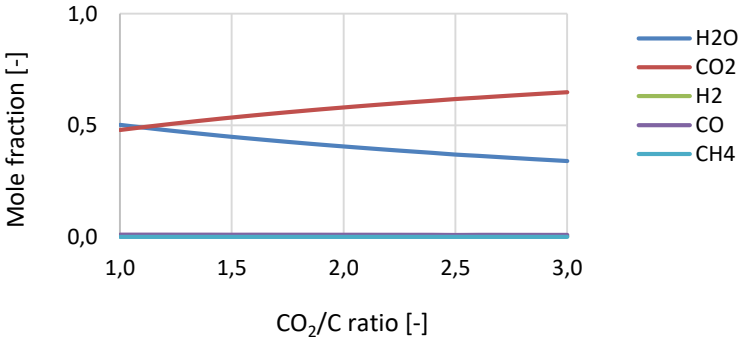

(b) OC/C ratio of 2

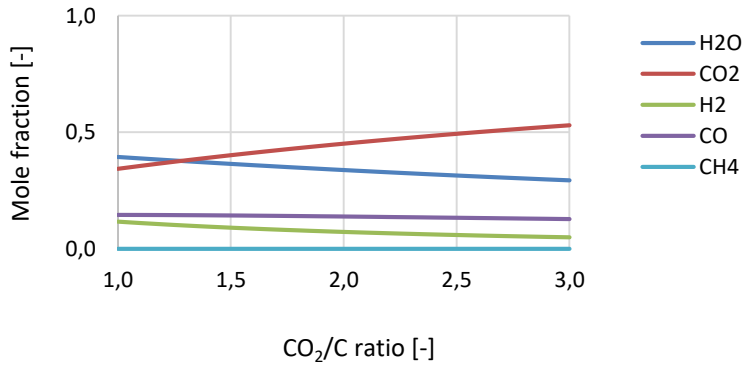

(C) OC/C ratio of 1

Figure 4-10 Effect of CO_2/C ratio on CLC using CuO with different OC/C ratios at Steam/C ratio of 2 and 950 °C.

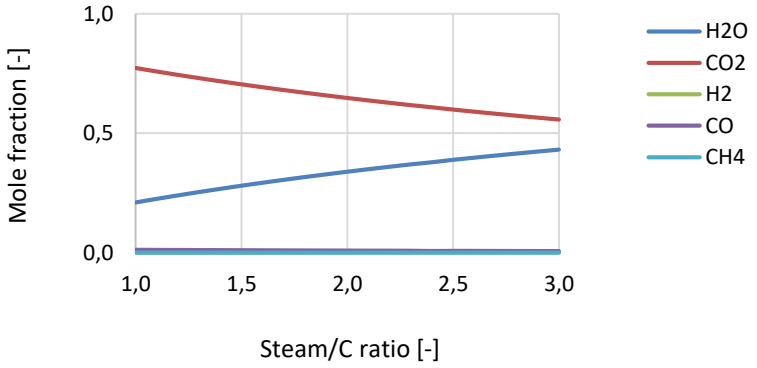

(a) CO_2/C ratio of 3

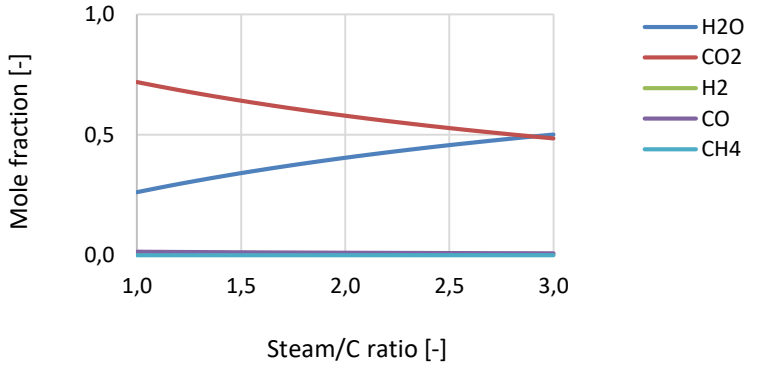

(b) CO_2/C ratio of 2

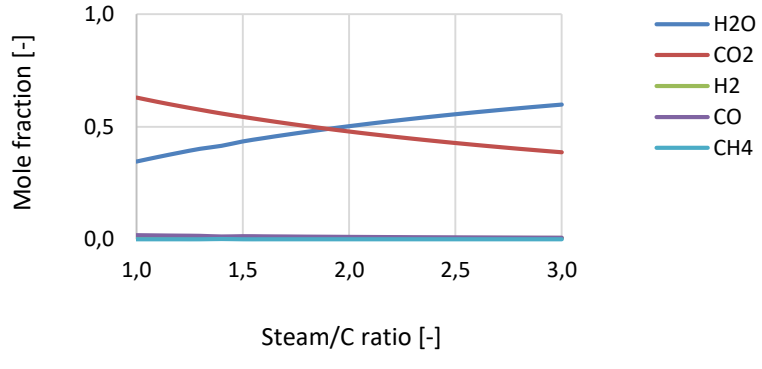

(C) CO_2/C ratio of 1

Figure 4-11 Effect of Steam/C ratio on CLC using CuO with different CO_2/C ratios at OC/C ratio of 2 and 950 °C.

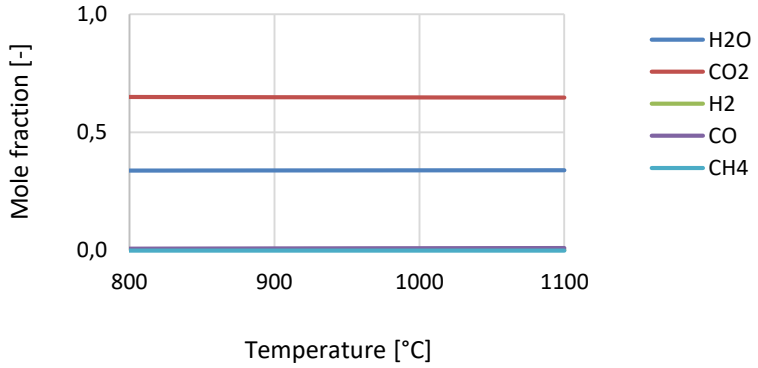

(a) CO_2/C ratio of 3

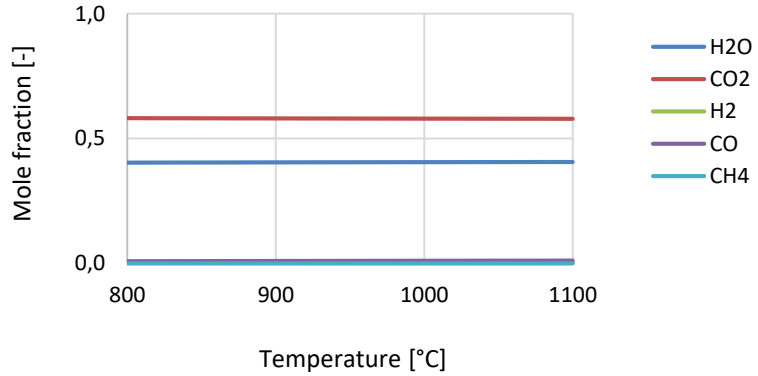

(b) CO_2/C ratio of 2

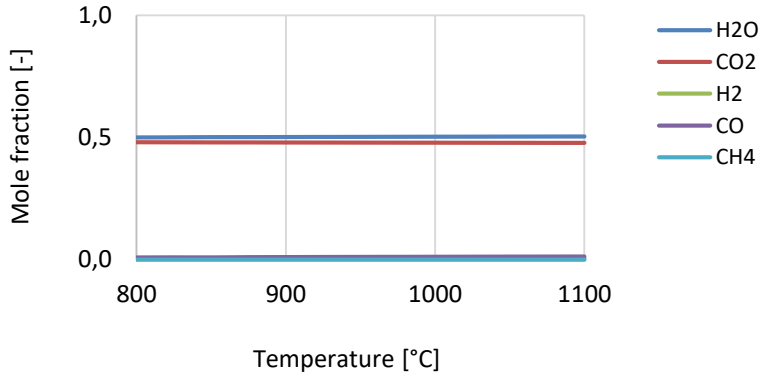

(C) CO_2/C ratio of 1

Figure 4-12 Effect of temperature on CLC using CuO with different CO_2/C ratios at OC/C ratio of 2 and Steam/C ratio of 2.

4.3.2 Estimation of available heat and produced power in a 3 MWth unit

The estimation for the available heat and produced power using equilibrium calculations for the 3 MW_{th} unit are presented in this section. As explained in Section 4.2, the fuel reactor is modelled using two sections, where the first one corresponds to the gasification reactions and the second one to the combustion with the oxygen carrier. Section 4.3.2.1 contains the equilibrium results for petcoke gasification and Section 4.3.2.2 shows the equilibrium results for the combustion with oxygen carrier and equilibrium conversions, which are used for the mass and energy balance in Section 4.3.2.3 .

The calculation basis and assumptions are described in detail in Section 4.2.2.

4.3.2.1 Gasification equilibrium results

As described in Section 4.2.2.1 , the fuel reactor is modelled as two sections, and in the first section petcoke is gasified with steam and CO_2 to produce the gasified fuel. Table 4-4 shows the equilibrium composition of gasification products of petcoke at 950 °C for 3 MW_{th} (321.76 kg/h of petcoke), with 77281 mol/h of a 50 % mol steam/CO_2 flow[5], using the minimization of the Gibbs free energy approach described in Section 4.2.1.1 . Table 4-3 shows the element balance considering steam, CO_2 and petcoke.

Table 4-3: Source of C, H, and O fed to the fuel reactor from steam, CO_2 and petcoke.

	Origin			Total flow
Element	H_2O	CO_2	Petcoke	[mol/h]
C	0	38640	26161	64802
H	77281	0	4431	81711
O	38640	77281	212	116134

Table 4-4 shows the equilibrium composition of the gasified fuel which is used as a feed to the mass and energy balance with the oxygen carrier (second lump).

Table 4-4: Equilibrium composition of gasification products of petcoke at 950°C

Species	Flowrate [mol/h]	Composition [%mol]
carbon	0.0	0.00 %
H_2O	22127.3	20.94 %
CO_2	29204.9	27.64 %
H_2	18727.9	17.73 %
CO	35596.5	33.69 %
CH_4	0.3	0.00 %

With the values in Table 4-4, 36 % of the C in petcoke is gasified with CO_2, while 64 % is gasified with H_2O. The endothermic enthalpy of the gasification is 1.06 MW. Note that in these calculations *no* oxygen carrier

[5] As mentioned in Section 4.2.2.2 , this is estimated from 1859 Nm^3/h at NPT (20 °C and 101.3 kPa) from the CHEERS pre-FEED study [2].

is included and these were used to estimate the flows of a gaseous stream for a mass and energy balance, as described in Section 4.2.2.1 .

4.3.2.2 *Chemical looping combustion equilibrium results*

Table 4-5 shows the molar flows to the fuel reactor used for equilibrium calculations. As described in Section 4.2.2, the calculations are done for a 3 MW_{th} unit, with 321.76 kg/h of petcoke and 77281 mol/h of a 50 % mol steam/CO_2 flow for fluidization and gasification[6]. The flows of metal oxide are calculated as the stochiometric flow of oxygen carrier to produce CO_2 and H_2O from the C and the H in petcoke. Note that the element feed from petcoke, H_2O and CO_2 is the same as in Table 4-3.

Table 4-5: Feed to fuel reactor for equilibrium calculations for 3 MW_{th} mass and energy balance

Oxygen carrier system	Elements fed to FR from petcoke, H_2O and CO_2 [mol/h]			Metal Oxide [mol/h]				
	C	H	O	Fe_2TiO_5	TiO_2	CuO	NiO	Fe_2O_3
Ilmenite	64802	81711	116134	54325	54325	0	0	0
Fe_2O_3/Fe_3O_4	64802	81711	116134	0	0	0	0	162976
Cu/CuO	64802	81711	116134	0	0	54325	0	0
Ni/NiO	64802	81711	116134	0	0	0	54325	0

The element balance used as constraint for the equilibrium calculations is obtained from Table 4-5 and is shown in Table 6-1 in the **APPENDIX** (Section 6.4) .

Table 4-6 shows the equilibrium flows in the FR, obtained with the minimization of the Gibbs free energy approach described in Section 4.2.1.1 , considering the feed to the fuel reactor in section 4.2.1 at 950°C.

Table 4-6: Equilibrium flows and conversions for combustion of petcoke with different oxygen carriers

	Ilmenite	Cu/CuO	Ni/NiO	Fe_2O_3/Fe_3O_4
Equilibrium flows [mol/h]				
Carbon	7	0	0	0
H_2O	38472	40814	40856	40851
CO_2	59487	64708	64801	64791
H_2	2384	41	0	5
CO	5308	94	0	11
CH_4	0	0	0	0
Oxidized OC	15412	135	1	48
Reduced OC	93240	54190	54325	108619

[6] As explained in Section, 4.2.2.2 , this is estimated from 1859 Nm^3/h at NPT (20 °C and 101.3 kPa) from the CHEERS pre-FEED study [2].

The conversions of CO and H_2 in Table 4-7 are calculated based on the equilibrium flowrates and are used as input to the mass and energy balance model.

Table 4-7: Conversions for combustion of petcoke with different oxygen carriers

	Ilmenite	Cu/CuO	Ni/NiO	Fe_2O_3/Fe_3O_4
Conversions [%]				
CO	85.1	99.7	100.0	100.0
H_2	87.3	99.8	100.0	100.0

4.3.2.3 Estimation of recovered heat and produced power using equilibrium calculations

The results from the estimation of power production for ilmenite and Ni/NiO are shown in Table 4-8. Since CuO and iron oxide have very similar stoichiometric equilibrium conversions to NiO, only one of these oxygen carriers was included in the calculations. These results are obtained using the approach and assumptions described in Section 4.2.2, the feed composition in Table 4-4 and the conversions in Table 4-7.

Table 4-8: Results from estimation of power production potential for 3MW_{th} case

Parameter	Ilmenite (stoichiometric OC)	Ilmenite (20 % excess OC)	Ni/NiO (stoichiometric OC)
Thermal energy input [MW]	3.00	3.00	3.00
Fuel reactor temperature [°C]	927	952	947
Oxygen carrier flow rate [kg/s]	3.60	4.19	5.45
AR cooling [MW]	0.86	1.26	1.27
Available AR + FR exhaust heat [MW]	1.51	1.47	1.46
Total available heat [MW]	2.36	2.73	2.73
Power production from AR [MW]	0.33	0.49	0.49
Power production from gases [MW]	0.48	0.47	0.46
Total power production [MW]	0.81	0.95	0.96
Power produced/available heat (%)	34.25	34.94	34.94
Power produced/energy input (%)	26.99	31.77	31.84

As can be seen from the table, the Ni/NiO case has larger amounts of available heat than ilmenite with stochiometric feed of OC, primarily due to the higher conversion. This results in increased power production from the CLC system. However, Ni/NiO is toxic and less accessible than ilmenite. Moreover, complete combustion can be achieved when feeding ilmenite "in excess", achieving performance as with Ni/NiO. This is expected as the boundary conditions in the cases with complete combustions are similar for the different oxygen carriers - same thermal energy input as petcoke, same oxygen requirement based on stoichiometry while the difference is in the flow rate/circulation of oxygen carriers.

An interesting result is the oxygen carrier flow rate for the three cases. For the stoichiometric oxygen carrier case, the flow rate of the active Me/MeO part for the ilmenite will be greater than that of Ni/NiO system

as it has a higher molecular weight. However, the Ni/NiO system only has 18 % of active material. The remainder 82 % is support material made of alumina. In the case of ilmenite, only the active species are considered. Thus, the flow rate of oxygen carrier for the ilmenite cases, both for the stochiometric oxygen carrier and the 20 % excess cases is lower than that for the Ni/NiO system, while for a system consisting only of active Me/MeO in the process the Ni/NiO case will have a lower flow rate than ilmenite. The lower OC flow rate points towards a more compact process with reduced CAPEX. It should be noted that the ilmenite will typically have inerts which will increase the flow rate and that the ratio of support to active material in the Ni/NiO system is based on values from literature that were not necessarily optimised for the process.

It should be noted that these are punctual results (for one operating point) and a parametric analysis within the mass and energy balance would provide a wider perspective of the effect of varying operating conditions for different oxygen carriers and information for selecting a convenient operating point for each oxygen carrier.

4.4 Final comments

The framework developed within this deliverable can be used to analyse different oxygen carrier systems of interest for CLC. This approach can be used as part of the evaluation of the convenience of further analysing potential oxygen carriers for CLC. The actual process performance will also be affected by the kinetic behaviour of the oxygen carrier and reactor design, especially during gasification, which may be considered for improving the model in a future stage. However, the insights given by the presented equilibrium analysis can be used to establish targets for process performance, to propose operating conditions and in general, to improve the understanding of the effect of varying operating conditions with different oxygen carriers. For instance, this work highlighted the requirement for excess oxygen carrier in the ilmenite case for complete combustion of petcoke.

Section 4 of this deliverable includes a parametric analysis for equilibrium composition in the fuel reactor, varying parameters of interest such as steam flow, steam/CO_2 ratio and temperature. In addition, an example of the mass and energy balance results using equilibrium conversion for two different oxygen carrier systems is included in this section. This analysis can be extended by performing a parametric analysis also on the mass and energy balance to estimate the potential for power production.

5 REFERENCES

[1] Toomey R. and Johnstone H.P., Chemical Engineering Progress, 48 (1952) 220-226.

[2] Davidson J.F. and Harrison D.H., Fluidised Particles, Cambridge University Press, Cambridge 1963.

[3] Wen C.Y. and Fan L.T., Models for Flow Systems and Chemical Reactors, Marcel Dekker, New York 1975.

[4] Kunii Daizo and Levenspiel Octave, Fluidization Engineering, Butterworth-Heinemann, Boston 1991.

[5] Kunii D. and Levenspiel O., Bubbling Bed Model, Ind Eng Chem Fund, 7 (1968) 446-452.

[6] Werther J., Chem. Ing. Tech., 49 (1977) 777-785.

[7] J. Werther and J. Wein, "Expansion behavior of gas fluidized bed in the turbulent regime," A.I.Ch.E. Symposium Series, vol. 90, no. 301, pp. 31–44, 1994.

[8] Wytrwat T., Fluid dynamics of turbulent fluidized beds for particles of Geldart group B, Hamburg University of Technology 2020

[9] Foka M., Chaouki J., Guy C. and Klvana D., Gas phase hydrodynamics of a gas-solid turbulent fluidized bed reactor, Chemical Engineering Science, 51(1996), 713-723

[10] Thompson M. L., Bi H. and Grace J. R., A generalized bubbling/turbulent fuidized-bed reactor model, Chemical Engineering Science, 54 (1999) 2175-2185

[11] LEE G. S. and KIM S. D., Axial Mixing of Solids in Turbulent Fluidized Beds, The Chemical Engineering Journal, 44 (1990) 1 - 9

[12] Foka M., Chaouki J., Guy C. and Klvana D., Gas phase hydrodynamics of gas-solid turbulent fluidized bed reactor, Chemical Engineering Science, 51 (1996) 713-723

[13] Vepsäläinen A., Heterogeneous mass transfer in fluidized beds by computational fluid dynamics, Lappeenranta University of Technology

[14] Thompson M. L., Bi H. and Grace J. R., A generalized bubbling/turbulent fluidized-bed reactor model, Chemical Engineering Science 54 (1999) 2175}2185

[15] VDI heat atlas second edition, VDI-Gesellschaft Verfahrenstechnik und Chemieingenieurwesen, DOI 10.1007/978-3-540-77877-6

[16] Monazam E. R., Panday R. and Shadle L. J., Estimate of Solid Flow Rate from Pressure Measurement in Circulating Fluidized Bed, Powder technology 203(1) (2010) 91-97

[17] Blasius H., Das Ähnlichkeitsgesetz bei Reibungsvorgängen in Flüssigkeiten, Mitteilungen der Forschungen des Verein Deutscher Ingenieure (VDI), 131 (1913) 1-39

[18] D. Douchanov and G. Angelova, "Effect of catalysis and inlet gas on coal gasification," *Fuel*, vol. 62, no. 2, pp. 231–233, Feb. 1983.

[19] S. Tebianian *et al.*, "'D2.3 Pre-FEED for the demonstrator' CHEERS project report," 2019.

[20] S. Kang and Z. Lei, "Measurement of the thermodynamic properties of Fe2Ti3O9 and Fe2TiO5," *Trans. NFsoc*, vol. 6, no. 1, pp. 25–31, 1996.

[21] H. Leion, A. Lyngfelt, M. Johansson, E. Jerndal, and T. Mattisson, "The use of ilmenite as an oxygen carrier in chemical-looping combustion," *Chem. Eng. Res. Des.*, vol. 86, no. 9, pp. 1017–1026, Sep. 2008.

[22] S. Nagpal, T. K. Sarkar, and P. K. Sen, "Simulation of petcoke gasification in slagging moving bed reactors," *Fuel Process. Technol.*, vol. 86, no. 6, pp. 617–640, Mar. 2005.

[23] P. V. Suresh, K. G. Menon, K. S. Prakash, S. Prudhvi, and A. Anudeep, "Thermodynamic analysis of in situ gasification-chemical looping combustion (iG-CLC) of Indian coal," *Environ. Sci. Pollut. Res.*, vol. 23, no. 20, pp. 20111–20119, Oct. 2016.

[24] A. Lima da Silva, C. de F. Malfatti, and I. L. Müller, "Thermodynamic analysis of ethanol steam reforming using Gibbs energy minimization method: A detailed study of the conditions of carbon deposition," *Int. J. Hydrogen Energy*, vol. 34, no. 10, pp. 4321–4330, May 2009.

[25] C. C. Sreejith, P. Arun, and C. Muraleedharan, "Thermochemical Analysis of Biomass Gasification by Gibbs Free Energy Minimization Model—Part: I (Optimization of Pressure and Temperature)," *Int. J. Green Energy*, vol. 10, no. 3, pp. 231–256, Mar. 2013.

[26] S. Shabbar and I. Janajreh, "Thermodynamic equilibrium analysis of coal gasification using Gibbs energy minimization method," *Energy Convers. Manag.*, vol. 65, pp. 755–763, Jan. 2013.

[27] W. B. White, S. M. Johnson, and G. B. Dantzig, "Chemical Equilibrium in Complex Mixtures," *J. Chem. Phys.*, vol. 28, no. 5, pp. 751–755, May 1958.

[28] A. Wächter and L. T. Biegler, "On the implementation of an interior-point filter line-search algorithm for large-scale nonlinear programming," *Math. Program.*, vol. 106, no. 1, pp. 25–57, Mar. 2006.

[29] J. A. E. Andersson, J. Gillis, G. Horn, J. B. Rawlings, and M. Diehl, "CasADi: a software framework for nonlinear optimization and optimal control," *Math. Program. Comput.*, vol. 11, no. 1, pp. 1–36, Mar. 2019.

[30] "Find minimum of constrained nonlinear multivariable function (fmincon)," *Matlab Documentation*. [Online]. Available: http://www.mathworks.se/help/optim/ug/fmincon.html.

[31] "FactSage," *The Integrated Thermodynamic Databank System*, 2020. [Online]. Available: www.factsage.com/.

[32] D. Rohde, T. Andresen, C. Zotica, and P. Wilpert, "Energy Recovery From Furnace Off-Gas: Analysis of

an Integrated Energy Recovery System by Means of Dynamic Simulation," *To Appear Int. J. Refrig.*, 2020.

[33] M. Yang, Y. long Zhou, D. Wang, J. Han, and Y. Yan, "Thermodynamic cycle analysis and optimization to improve efficiency in a 700 °C ultra-supercritical double reheat system," *J. Therm. Anal. Calorim.*, vol. 141, no. 1, pp. 83–94, 2020.

[34] Y. Larring, Z. Li, A. Tilland, and A. Lambert, "'D3.1b: Selection of the 1st oxygen carrier and characterization of its most critical properties' CHEERS Project report," 2018.

[35] The SciPy community, "SciPy minimize." [Online].
Available: https://docs.scipy.org/doc/scipy/reference/generated/scipy.optimize.minimize.html.

6 APPENDIX

6.1 Effect of CO_2/steam ratio with NiO

6.1.1 Effect of OC/C ratio on CLC using NiO with varying CO_2/C ratios

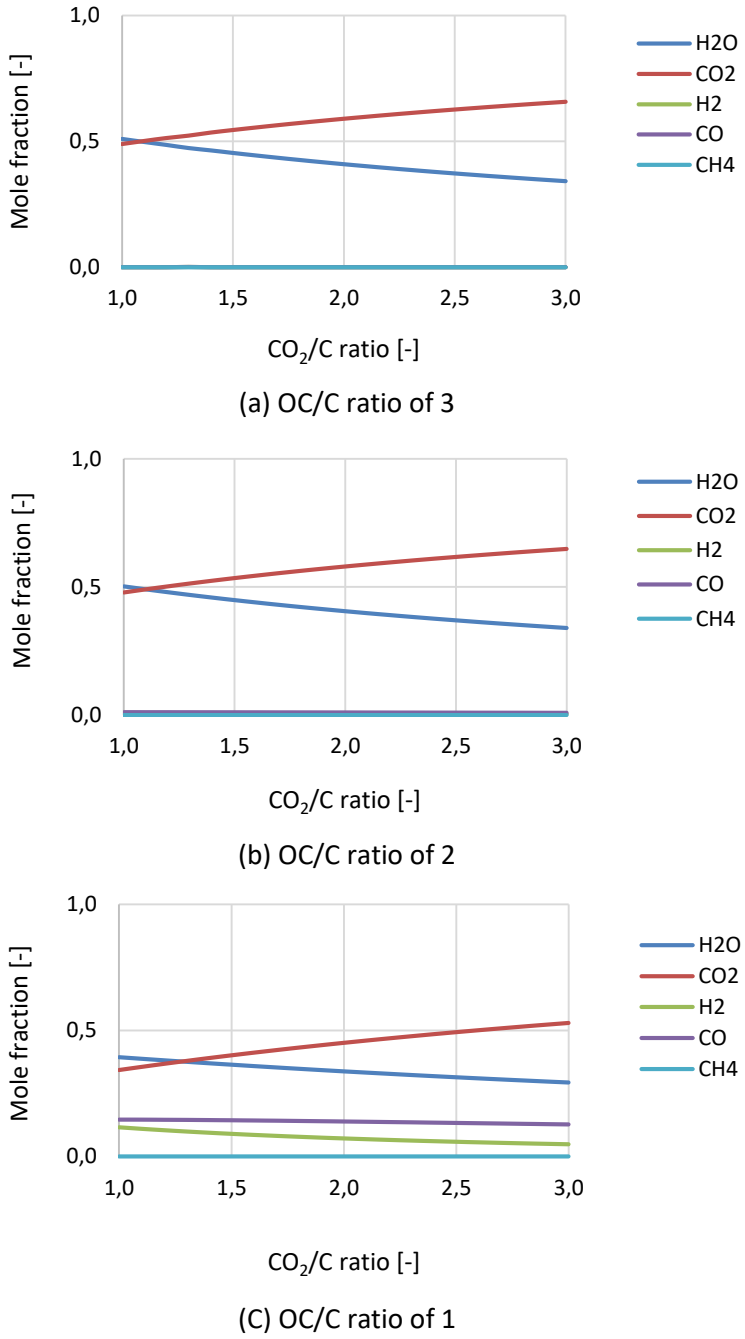

Figure 6-1 Effect of CO_2/C ratio on CLC using NiO with different OC/C ratios at Steam/C ratio of 2 and 950 °C.

6.1.2 Effect of CO_2/C ratio on CLC using NiO with varying Steam/C ratios

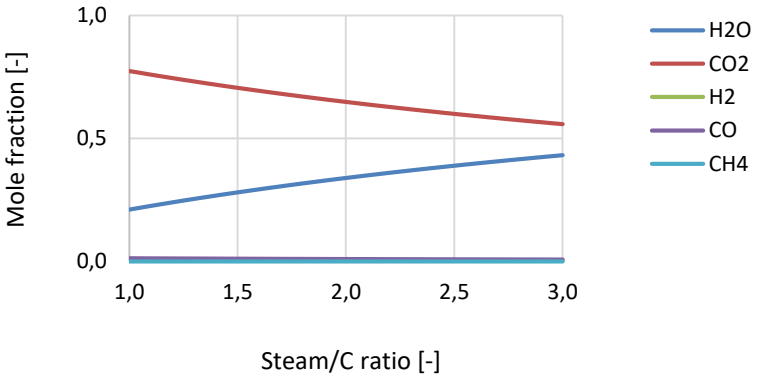

(a) CO_2/C ratio of 3

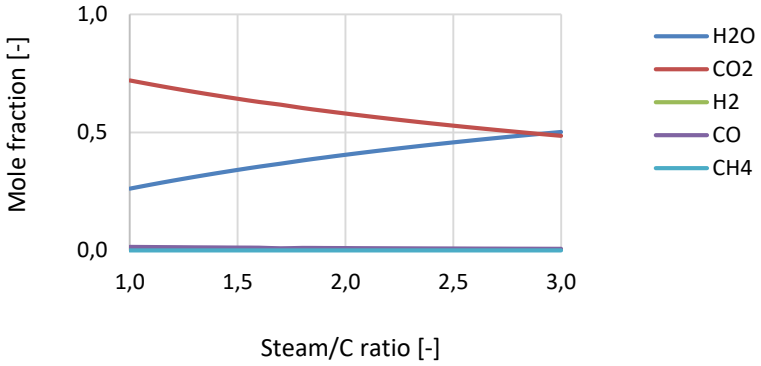

(b) CO_2/C ratio of 2

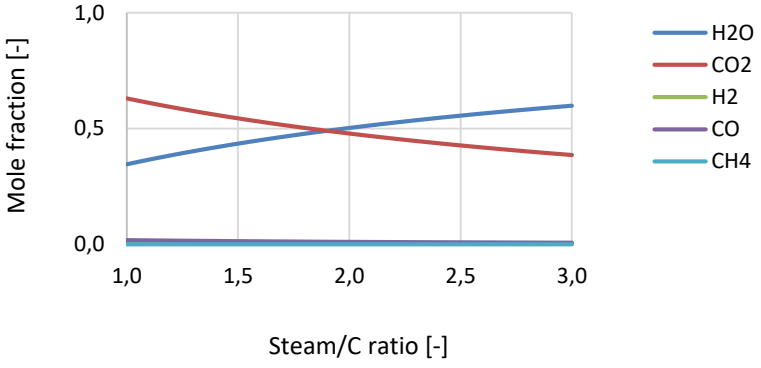

(C) CO_2/C ratio of 1

Figure 6-2 Effect of Steam/C ratio on CLC using NiO with different CO_2/C ratios at OC/C ratio of 2 and 950 °C.

6.1.3 Effect of CO_2/C ratio on CLC using NiO with varying temperatures

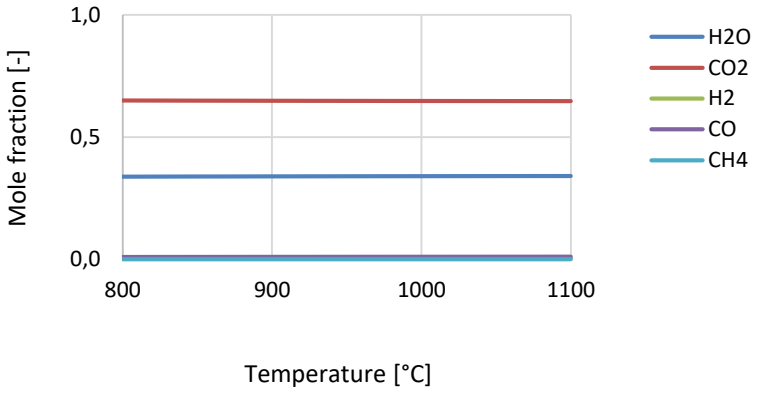

(a) CO_2/C ratio of 3

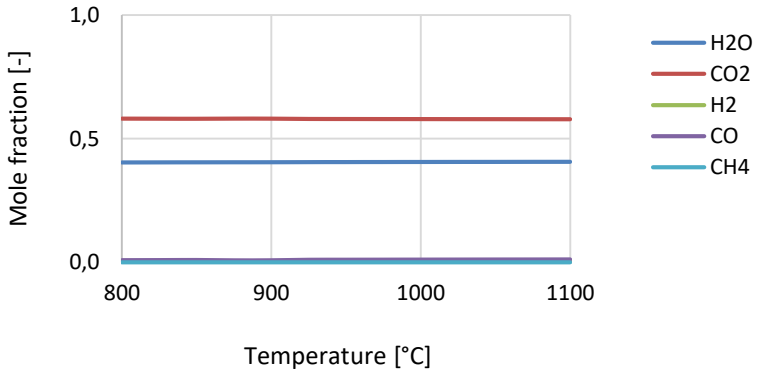

(b) CO_2/C ratio of 2

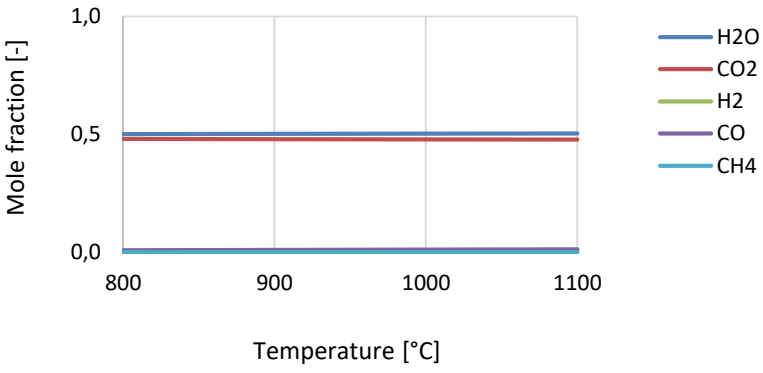

(C) CO_2/C ratio of 1

Figure 6-3 Effect of temperature on CLC using NiO with different CO_2/C ratios at OC/C ratio of 2 and Steam/C ratio of 2.

6.2 Effect of CO_2/steam ratio with Fe_2O_3

6.2.1 Effect of OC/C ratio on CLC using Fe_2O_3 with varying CO_2/C ratios

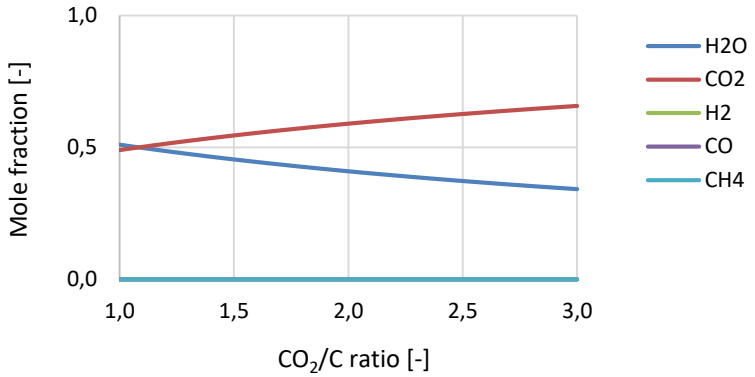

(a) OC/C ratio of 9

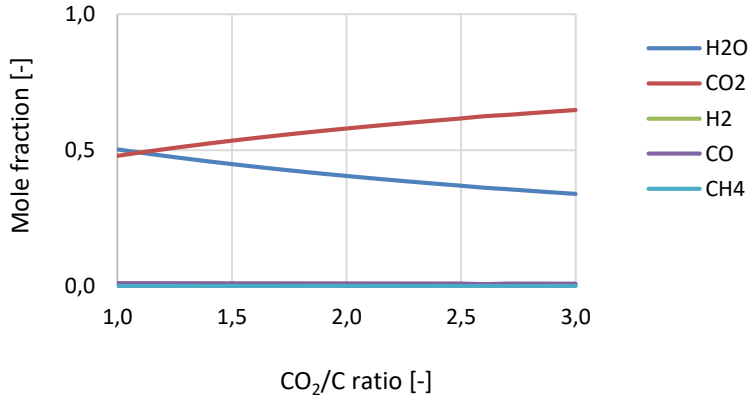

(b) OC/C ratio of 6

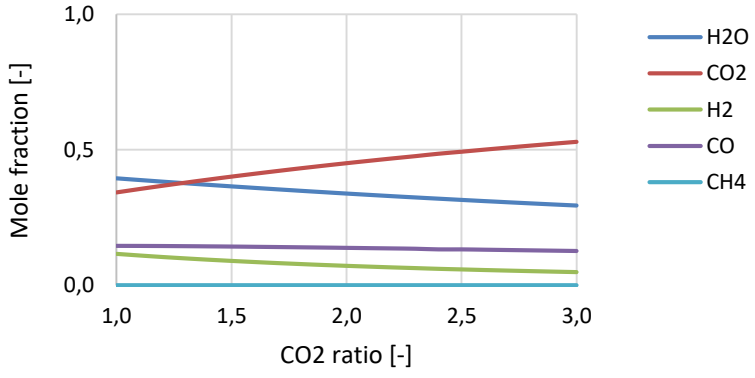

(C) OC/C ratio of 3

Figure 6-4 Effect of CO_2/C ratio on CLC using Fe_2O_3 with different OC/C ratios at Steam/C ratio of 2 and 950 °C.

6.2.2 Effect of CO_2/C ratio on CLC using Fe_2O_3 with varying Steam/C ratios

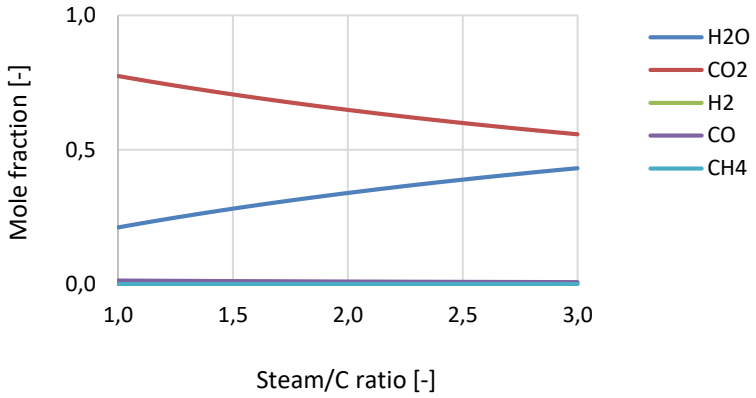

(a) CO_2/C ratio of 3

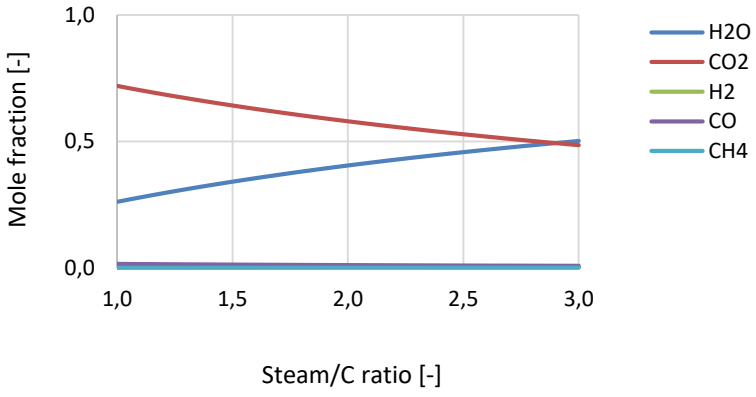

(b) CO_2/C ratio of 2

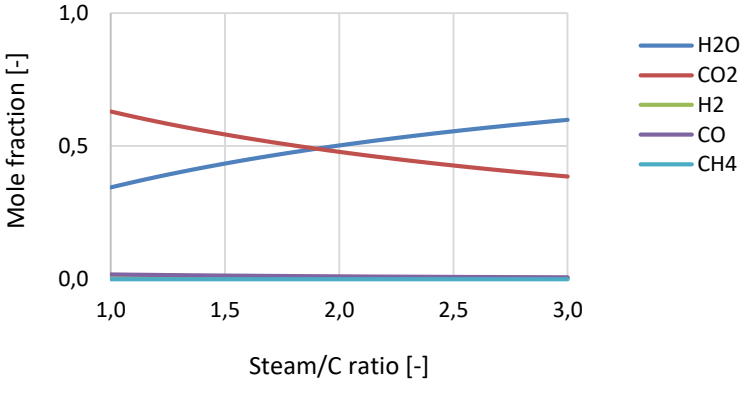

(C) CO_2/C ratio of 1

Figure 6-5 Effect of Steam/C ratio on CLC using Fe_2O_3 with different CO_2/C ratios at OC/C ratio of 6 and 950 °C.

6.2.3 Effect of CO_2/C ratio on CLC using Fe_2O_3 with varying temperatures

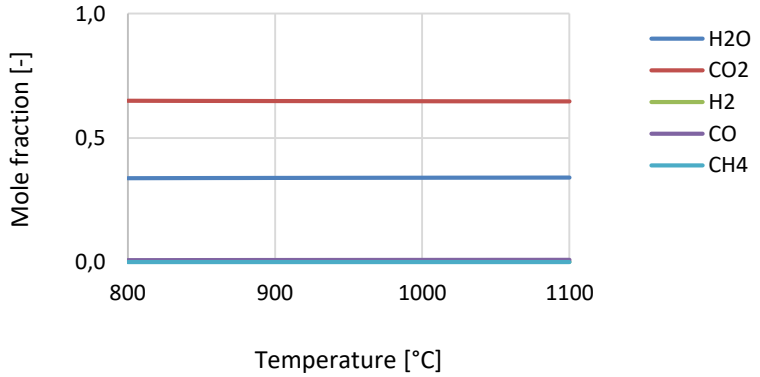

(a) CO_2/C ratio of 3

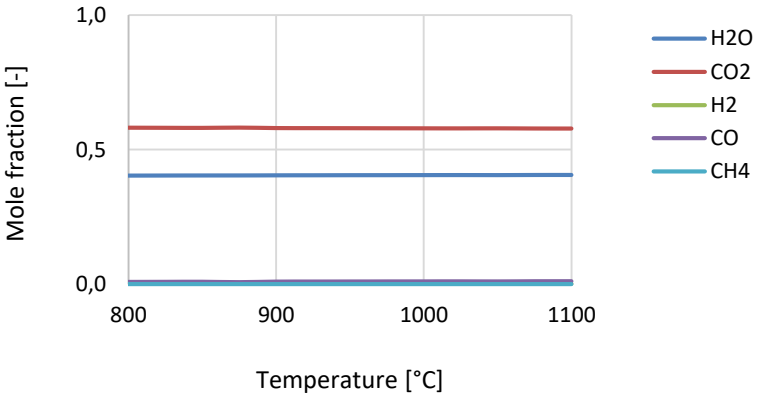

(b) CO_2/C ratio of 2

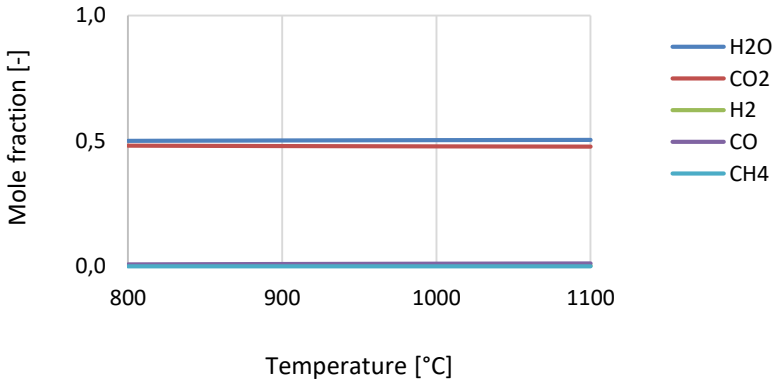

(C) CO_2/C ratio of 1

Figure 6-6 Effect of temperature on CLC using Fe_2O_3 with different CO_2/C ratios at OC/C ratio of 6 and Steam/C ratio of 2.

6.3 Effect of CO_2/steam ratio with ilmenite

6.3.1 Effect of OC/C ratio on CLC using ilmenite with varying CO_2/C ratios

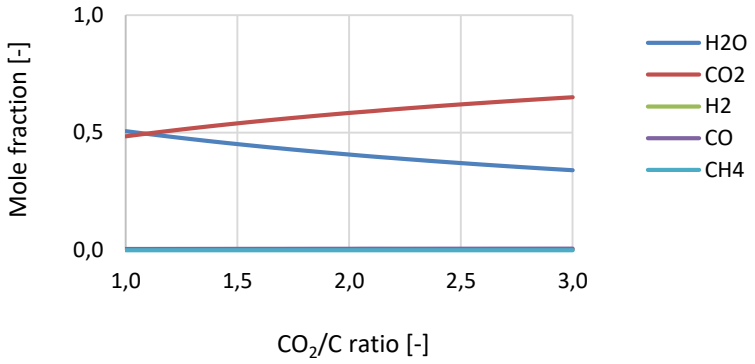

(a) OC/C ratio of 3

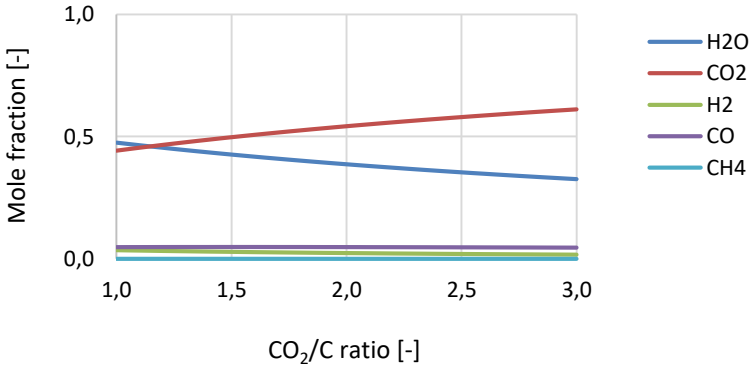

(b) OC/C ratio of 2

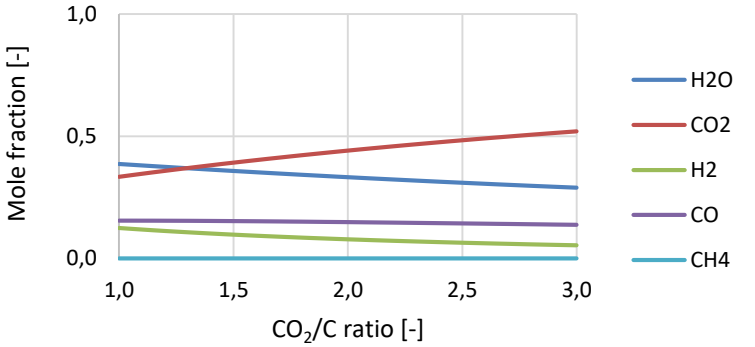

(C) OC/C ratio of 1

Figure 6-7 Effect of CO_2/C ratio on CLC using ilmenite with different OC/C ratios at Steam/C ratio of 2 and 950 °C.

6.3.2 Effect of CO_2/C ratio on CLC using ilmenite with varying Steam/C ratios

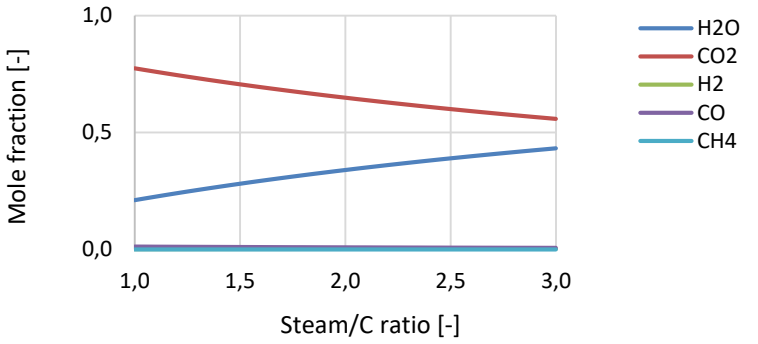

(a) CO_2/C ratio of 3

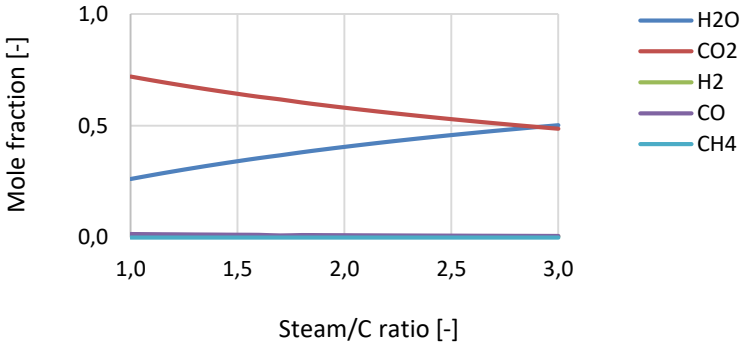

(b) CO_2/C ratio of 2

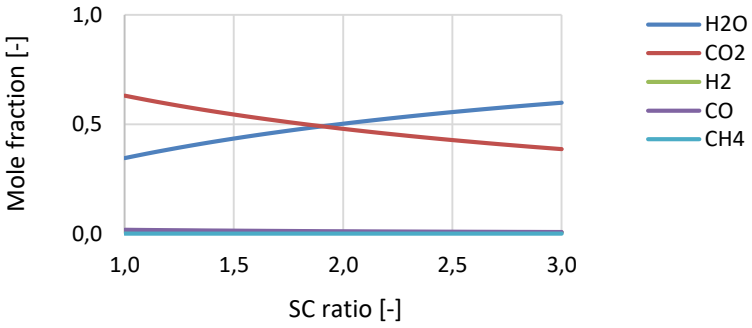

(C) CO_2/C ratio of 1

Figure 6-8 Effect of Steam/C ratio on CLC using ilmenite with different CO_2/C ratios at OC/C ratio of 2 and 950 °C.

6.3.3 Effect of CO_2/C ratio on CLC using ilmenite with varying temperatures

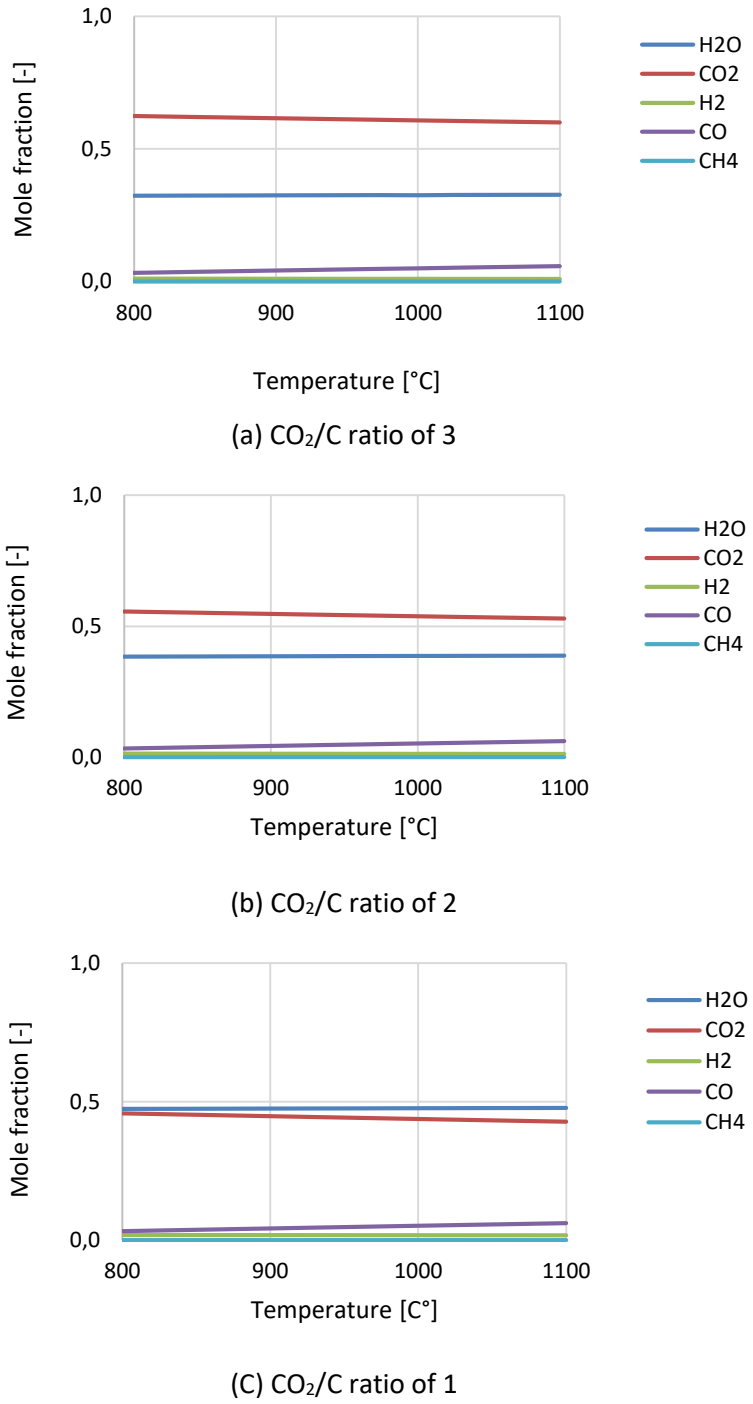

Figure 6-9 Effect of temperature on CLC using ilmenite with different CO_2/C ratios at OC/C ratio of 2 and Steam/C ratio of 2.

6.4 Feed to fuel reactor for equilibrium calculations

Table 6-1 shows the element balance for equilibrium calculations for the 3 MW_{th} case study (A_j in Equation 3 and Equation 4), based on the feed to the fuel reactor in Table 4-5 and at stoichiometric OC requirement. Note that the total flow of C and H in Table 4-3 (feed for gasification lump in FR) and Table 4-3 is the same, and the difference in O corresponds to the oxygen in the oxygen carrier.

Table 6-1. Constraints (element balance) for equilibrium calculations in fuel reactor for 3 MW_{th} mass and energy balance

Oxygen carrier	C [mol/h]	H [mol/h]	O [mol/h]	Fe [mol/h]	Ti [mol/h]	Cu [mol/h]	Ni [mol/h]
Ilmenite	64802	81711	496412	108651	108651	0	0
Fe_2O_3/Fe_3O_4	64802	81711	605063	325953	0	0	0
Cu/CuO	64802	81711	170459	0	0	54325	0
Ni/NiO	64802	81711	170459	0	0	0	54325